Available online at www.sciencedirect.com
ScienceDirect
Coordination Chemistry Reviews 251 (2007) 2145–2166
COORDINATION CHEMISTRY REVIEWS
www.elsevier.com/locate/ccr

Review

Metal–carbon multiple bonded complexes Carbene, vinylidene and allenylidene complexes of ruthenium and osmium supported by macrocyclic ligands

Chi-Ming Che *, Chi-Ming Ho, Jie-Sheng Huang

Department of Chemistry and Open Laboratory of Chemical Biology of the Institute of Molecular Technology for Drug Discovery and Synthesis, The University of Hong Kong, Pokfulam Road, Hong Kong, China

Received 28 October 2006; accepted 31 March 2007
Available online 5 April 2007

Contents

Abstract

In this review, we present our recent studies on the synthesis, structures, spectroscopic and electrochemical properties, and reactivities of ruthenium/osmium–carbon multiple bonded complexes. The first part of the review deals with the chemistry of ruthenium/osmium porphyrin carbene complexes and related metal carbene complexes (including iron porphyrin carbene complexes and ruthenium carbene complexes supported by salens or polypyridines). The second part describes the chemistry of ruthenium vinylidene and allenylidene complexes supported by macrocyclic tertiary amine ligands Me_3tacn (1,4,7-trimethyl-1,4,7-triazacyclononane) and 16-TMC (1,5,9,13-tetramethyl-1,5,9,13-tetraaza-cyclohexadecane).

Keywords: Metal–carbon multiple bonds; Macrocyclic ligands; Ruthenium complexes; Osmium complexes

1. Introduction

The study of metal–carbon multiple bonded complexes [1,2], such as carbene, vinylidene and allenylidene complexes of transition metals, continues to be an active area of research, as indicated by recent publication of a large number of review articles in this area [3] and a special issue of Coordination

* Corresponding author. Tel.: +852 28592154; fax: +852 28571586.
E-mail address: cmche@hku.hk (C.-M. Che).

0010-8545/$ – see front matter © 2007 Elsevier B.V. All rights reserved.
doi:10.1016/j.ccr.2007.03.019

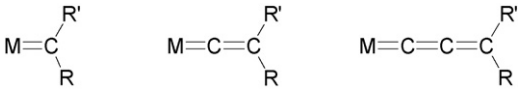

Fig. 1. Metal-carbon multiple bonded complexes described in this review (M = Ru, Os; in some case R = R′).

Chemistry Reviews on vinylidene, allenylidene, and metallacumulene complexes (vol. 248, issues 15–16, 2004). Our interest in metal–carbon multiple bonded complexes is largely focused on carbene, vinylidene and allenylidene complexes of ruthenium and osmium (Fig. 1). Such complexes are involved in a variety of important organic transformations catalyzed by ruthenium and osmium complexes. For instance, it is widely known that Grubb's ruthenium carbene complexes $[(L)_2Cl_2Ru{=}CHR]$ or $[(L)(L')Cl_2Ru{=}CHR]$ (L = tertiary phosphine, L′ = *N*-heterocyclic carbene) are highly active and selective catalysts for alkene metathesis reactions [4]. Ruthenium and osmium porphyrin carbene complexes are proposed to be the active intermediates in various C–C bond formation reactions and C–H insertion reactions promoted by ruthenium or osmium porphyrin catalysts [5,6]. Ruthenium vinylidene and alkenylidene complexes serve as catalyst precursors for alkene metathesis reactions and are the key intermediates in catalytic conversion of alkynes, including dimerization of terminal alkyne, cycloaromatization of conjugated enediynes and addition of oxygen, nitrogen and carbon nucleophiles to alkynes [3g,3q,3t]. Moreover, there have been exciting developments in metallacumulenes $M(=C)_nCR_2$ as novel non-linear optical materials and molecular wires in the past decade [3m,7].

Up to now, many ruthenium and osmium carbene, vinylidene and allenylidene complexes have been reported in the literature, the majority of which (excluding those bearing porphyrin macrocycles) are supported by carbonyl, phosphine or cyclopentadienyl ligands [1–3], some are supported by *N*-chelating ligands such as hydridotris(pyrazol-1-yl)borate and its derivatives [8a,8b]. Examples of ruthenium and osmium carbene, vinylidene and allenylidene complexes containing macrocyclic non-porphyrin ligands are sparse. Notable examples are ruthenium carbene complexes supported by dibenzotetramethyltetraaza[14]annulene [8c] and ruthenium vinylidene complexes supported by a porphyrinogen ligand [8d].

Our group mainly employed the macrocyclic ligands such as porphyrins (Por, Fig. 2), Me_3tacn and 16-TMC (Fig. 3) to support ruthenium– and osmium–carbon multiple bonds. Investigation on the chemistry of ruthenium and osmium porphyrin

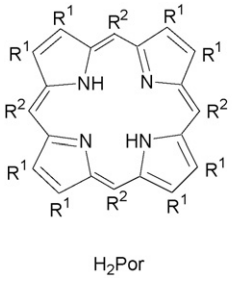

H_2Por

Por	R^1	R^2
TPP	H	Ph
TTP	H	4-MeC_6H_4
TMP	H	2,4,6-$Me_3C_6H_2$
4-X-TPP	H	4-XC_6H_4
2,6-Cl-TPP	H	2,6-$Cl_2C_6H_3$
3,4,5-MeO-TPP	H	3,4,5-$(MeO)_3C_6H_2$
F_{20}-TPP	H	C_6F_5
OEP	Et	H
D_4-Por*	H	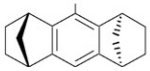

Fig. 2. Porphyrin abbreviations.

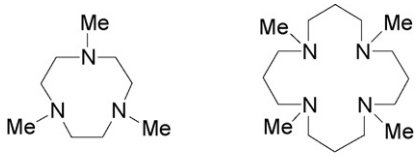

Me_3tacn 16-TMC

Fig. 3. Macrocyclic polyamine ligands.

carbene complexes would help understanding of the carbenoid transfer reactions catalyzed by ruthenium and osmium porphyrins [5,6]. The macrocyclic tertiary amine ligands Me_3tacn and 16-TMC are optically transparent in the UV–vis spectral region and are electrochemically silent, making these ligands well suitable for examination of electronic transitions associated with the $Ru(=C)_nCR_2$ moieties. In addition, Me_3tacn and 16-TMC ligands are σ-donors and do not complicate the π-bonding interactions between the metal ion and the $(=C)_nCR_2$ ligands.

This review describes our recent works on the synthesis, structures, spectroscopic and electrochemical properties, and reactivities of ruthenium/osmium–carbon multiple bonded complexes. The description is divided into two parts. The first part mainly deals with the chemistry of ruthenium/osmium carbene complexes of porphyrin ligands, together with iron porphyrin carbene complexes and ruthenium carbene complexes containing salen (tetradentate N_2O_2 Schiff-base dianions) or polypyridine ligands; the second part presents the chemistry of ruthenium vinylidene and allenylidene complexes supported by the macrocyclic tertiary amine ligands Me_3tacn and 16-TMC. We do not include here the ruthenium/osmium porphyrin carbene complexes reported before 2002 (unless they are needed for comparison); these complexes and their relevance to metal-mediated cyclopropanation of alkenes are the main topic discussed in our previous review [9].

2. Ruthenium and osmium carbene complexes supported by porphyrin ligands

2.1. Synthesis

Ruthenium and osmium porphyrin carbene complexes have been known for decades since the pioneering works of Collman and co-workers [10] and Woo and Smith [11]. These metal complexes can be prepared by several methods, including the following: (1) reaction of $[(TTP)M]_2$ (M = Ru or Os) with diazoalkanes or diazoesters, (2) treatment of monomeric [(TMP)Ru] with diazo compounds, (3) reaction of zero-valent ruthenium porphyrin dianion K_2[(TTP)Ru] with germinal dihalides Cl_2CHR ($R = CH_3$ or $SiMe_3$) and (4) treatment of [(Por)M(CO)] (M = Ru or Os) with diazo compounds [9].

By treating [(Por)Ru(CO)] with diazo compounds N_2CRR' under an inert atmosphere, we [12,13] prepared a wide variety of ruthenium porphyrin carbene complexes [(Por)Ru = CRR′] (**1**–**6**) and [(L)(Por)Ru = CRR′] (**7**–**10**) (Fig. 4), the latter are formed upon recrystallization of the former from solutions

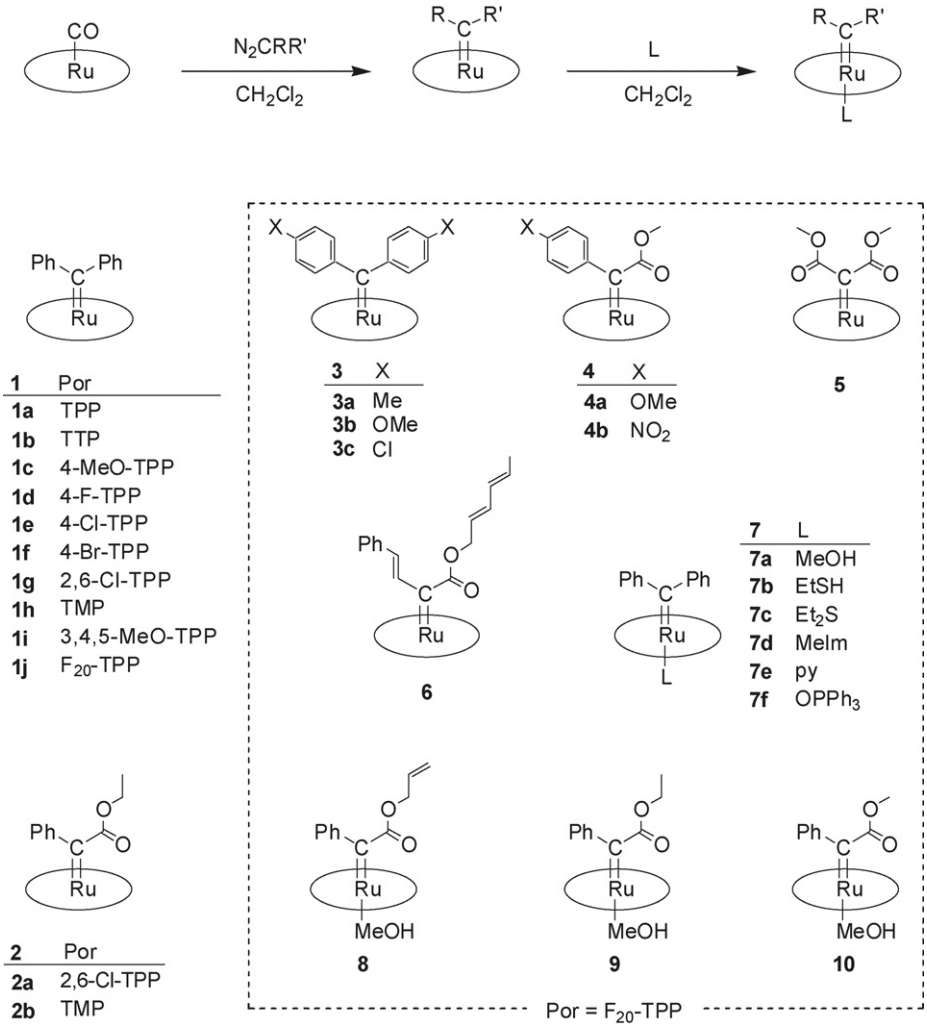

Fig. 4. Synthesis of ruthenium porphyrin carbene complexes **1**–**10** [12].

that contain molecules L such as MeOH, EtSH, Et_2S, 1-methylimidazole (MeIm) or pyridine (py). The formation of [(Por)Ru=CRR′] from [(Por)Ru(CO)] and N_2CRR' generally requires slow addition of the diazo compounds by syringe pump, to minimize the N_2CRR' decomposition reactions catalyzed by the ruthenium porphyrin complexes.

Simonneaux and co-workers observed that reaction of [(Por)Ru(CO)] with diisopropyldiazomethyl phosphonate $N_2CHP(O)(O^iPr)_2$ gives [(Por)Ru=CHP(O)(O^iPr)$_2$] (Por = TPP, TMP, F_{20}-TPP) [14], which are the first characterized examples of a phosphonate carbene complex.

Woo and co-workers obtained osmium porphyrin carbene complexes [(TTP)Os=CHR] (R = Mes, $CO_2CH_2CH_2CH_3$, 4-MeC_6H_4, 4-EtC_6H_4), [(TTP)Os=CMePh] and [(TTP)Os=C(CO_2Et){C(O)CH_2CH_2CH=CH_2}] by treating [Os(TTP)]$_2$ with N_2CHR (R = Mes, $CO_2CH_2CH_2CH_3$, 4-MeC_6H_4, 4-EtC_6H_4), N_2CMePh and $N_2C(CO_2Et)${C(O)CH_2CH_2CH=CH_2}, respectively, under nitrogen [5i].

According to a procedure similar to that for the preparation of [(MeIm)(F_{20}-TPP)Ru=CPh_2] (**7d**), we prepared osmium porphyrin carbene complex [(MeIm)(F_{20}-TPP)Os=CPh_2] (**11a**) starting from the reaction of [(F_{20}-TPP)Os(CO)] with N_2CPh_2 under an inert atmosphere [12]. Under aerobic conditions [(Por)Os(CO)] (Por = TPP, TTP, 4-F-TPP, 4-Cl-TPP, 4-Br-TPP) react with excess N_2CPh_2 at room temperature to give oxo-bridged osmium carbene complexes [{(Por)Os=CPh_2}$_2$(μ-O)] (**12a**–**e**, Fig. 5) [15], in contrast to the formation of bis-carbene complexes [(F_{20}-TPP)Os(=CPh_2)$_2$] from [(Por)Os(CO)] and excess N_2CPh_2 under similar conditions [16]. Probably, the electron-deficient nature of F_{20}-TPP plays a significant role in stabilizing the bis-carbene species. By employing electron-rich porphyrin ligand OEP, Miyamoto and co-workers [17] recently obtained [{(OEP)Os=CPh_2}$_2$(μ-O)] (a congener of **12a**–**e**) from

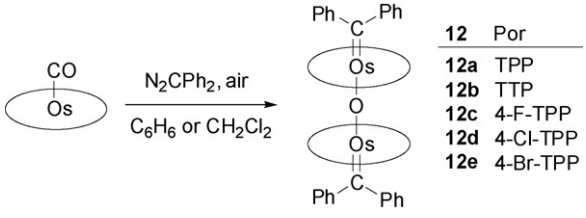

Fig. 5. Synthesis of oxo-bridged osmium porphyrin carbene complexes **12a**–**e** [15].

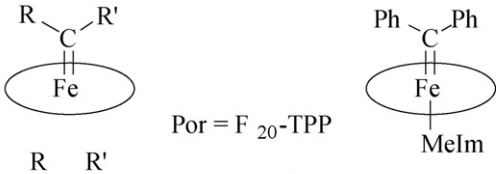

13	R	R'
13a	Ph	Ph
13b	Ph	CO_2Et
13c	Ph	$CO_2CH_2CH{=}CH_2$

14

Scheme 1. Structure formulae of **13a–c** and **14**.

the reaction of [(OEP)Os(CO)] with 1 equiv. of N_2CPh_2 in air. We found that the μ-oxo bridge in **12** can be cleaved by treating these complexes with pyridine. For example, reaction of **12b** with pyridine affords [(py)(TTP)Os=CPh_2] (**11b**) [15].

In view of the periodic relationship of ruthenium and osmium with iron, it would be of interest to compare the carbene complexes of these three transition metals. We reported that treatment of [Fe(F_{20}-TPP)] with diazo compounds N_2CPh_2, $N_2C(Ph)CO_2Et$ and $N_2C(Ph)CO_2CH_2CH{=}CH_2$ leads to the isolation of iron porphyrin carbene complexes [(F_{20}-TPP)Fe=CPh_2] (**13a**), [(F_{20}-TPP)Fe=$C(Ph)CO_2Et$] (**13b**) and [(F_{20}-TPP)Fe=$C(Ph)CO_2CH_2CH{=}CH_2$] (**13c**), respectively [18]. Complex **13a** readily binds MeIm to give a six-coordinate complex [(MeIm)(F_{20}-TPP)Fe=CPh_2] (**14**) (Scheme 1). These are the rare examples of isolable iron porphyrins bearing nonheteroatom-stabilized carbenes or (alkoxycarbonyl)carbenes, despite the report of many iron porphyrin carbene complexes (particularly those containing halo carbenes CX_2, CXX′ and CRX) since the pioneering work by Mansuy and co-workers [19]. Woo and co-workers observed the formation of [(TPP)Fe=CHR] (R = 2,4,6-$Me_3C_6H_2$ or $SiMe_3$) in the reaction of [Fe(TPP)] with diazo compounds; the Fe=CHR complexes are characterized by ^{1}H NMR spectroscopy and have not been isolated in pure form [20], probably due to their instability.

Diazo compounds are also a good carbene source for the preparation of ruthenium carbene complexes supported by salen ligands. Slow addition of N_2CR_2 (R = Ph, 4-$MeOC_6H_4$) to a series of chiral [Ru(salen)(PPh_3)$_2$] complexes affords chiral ruthenium carbene complexes [(salen)Ru=CR_2] (R = Ph or 4-$MeOC_6H_4$, respectively) [21], which, like [(salen)Ru(CO)], have a low solubility in common organic solvents such as MeOH, $CHCl_3$ and CH_2Cl_2. In the presence of MeIm or py, the solubility of [(salen)Ru=CR_2] in CH_2Cl_2 is dramatically enhanced, resulting in the formation of six-coordinate carbene complexes [(L)(salen)Ru=CR_2] (L = MeIm, py) (**15a–e**) [21] (Scheme 2).

Ruthenium carbene complexes of polypyridines can be prepared from the reaction of coordinated acetylide groups with alcohols. Treatment of [Ru(tpy)(bpy)(C≡CR^1)]$^+$ (tpy = 2,2′:6′,2″-terpyridine, bpy = 2,2′-bipyridine; R^1 = 4-$MeOC_6H_4$ or ^{t}Bu) with R^2OH (R^2 = Me, Et) under acidic conditions (by addition of CF_3COOH or HCl) gives [(tpy)(bpy)Ru=$C(OR^2)CH_2R^1$](ClO_4)$_2$ (**16a–c**) [22] (Scheme 3).

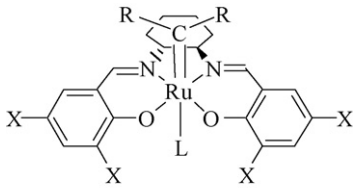

15	X	R	L
15a	Cl	Ph	MeIm
15b	Br	Ph	MeIm
15c	I	Ph	MeIm
15d	Br	Ph	py
15e	Br	4-$MeOC_6H_4$	MeIm

Scheme 2. Structure formulae of **15a–e**.

2.2. Spectroscopic features

All the ruthenium, osmium and iron carbene complexes **1–16** are diamagnetic species. Selected spectroscopic data of these complexes are listed in Table 1.

For the ruthenium and osmium porphyrin carbene complexes **1–12** [12,13,15], [(Por)Ru=CHP(O)(O^iPr)$_2$] (Por = TPP, TMP, F_{20}-TPP) [14] and [(TTP)Os=CRR′] [5i], their ^{1}H NMR spectra show the signals of H_β (the pyrrolic protons of the porphyrin ligands) at δ 8.13–8.6 (Ru) and 7.44–8.40 ppm (Os); the signals of the axial carbene groups (excluding the M=C*H*– signals if any) are significantly upfield from those of the corresponding diazo compound as a result of the porphyrin ring current effect. The M=C*H*– signals of [(Por)Ru=CHP(O)(O^iPr)$_2$] (Por = TPP, TMP, F_{20}-TPP) are located at δ 15.2–15.8 ppm [14] whereas those of [(TTP)Os=CHR] (R = Mes, $CO_2CH_2CH_2CH_3$, 4-MeC_6H_4, 4-EtC_6H_4) appear at δ 19.85–21.82 ppm [5i]. In the ^{13}C NMR spectra, the M=*C* signals appear at low fields with δ 280.49–346.69 (Ru) and 248–289.27 ppm (Os). Two Soret bands at $\lambda_{max} \approx 390$ and 425 nm are observed in the UV–vis absorption spectra of diarylcarbene complexes of ruthenium, whereas the other carbene complexes exhibit a single Soret band at λ_{max} 388–406 (Ru) and 398–418 nm (Os). The β bands of **1–12** appear at λ_{max} 519–538 nm.

We examined the effects of carbene substituents, porphyrin substituents, and trans ligands on the spectroscopic properties of

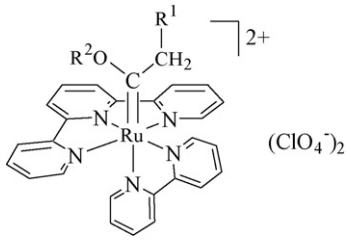

16	R^1	R^2
16a	4-$MeOC_6H_4$	Me
16b	^{t}Bu	Me
16c	4-$MeOC_6H_4$	Et

Scheme 3. Structure formulae of **16a–c**.

Table 1
Selected spectroscopic data of ruthenium and osmium carbene complexes

Complex	^{1}H NMR (δ (ppm))		^{13}C NMR (δ (ppm)) M=*C*	UV–vis (λ_{max} (nm)) (log ε)	Ref.
	H_β	M=C*H*–			
[(TPP)Ru=CPh_2] (**1a**)[a]	8.34 (s)		317.50	394 (5.07), 425 (4.96), 530 (4.26)	[12]
[(TTP)Ru=CPh_2] (**1b**)[a]	8.36 (s)		316.40	396 (5.08), 424 (4.94), 532 (4.20)	[12]
[(4-MeO-TPP)Ru=CPh_2] (**1c**)[a]	8.37 (s)		319.40	403 (5.08), 425 (4.93), 534 (4.27)	[12]
[(4-F-TPP)Ru=CPh_2] (**1d**)[a]	8.32 (s)		318.70	395 (5.01), 425 (4.92), 531 (4.26)	[12]
[(4-Cl-TPP)Ru=CPh_2] (**1e**)[a]	8.33 (s)		319.50	396 (5.00), 424 (4.91), 531 (4.25)	[12]
[(4-Br-TPP)Ru=CPh_2] (**1f**)[a]	8.33 (s)		319.70	396 (5.01), 427 (4.91), 531 (4.28)	[12]
[(2,6-Cl-TPP)Ru=CPh_2] (**1g**)[a]	8.17 (s)		327.86	390 (4.96), 430 (4.94), 533 (4.15), 560 (4.10)	[12]
[(TMP)Ru=CPh_2] (**1h**)[a]	8.13 (s)		318.08	395 (5.09), 430 (4.92), 534 (4.03), 562 (sh, 3.89)	[12]
[(3,4,5-MeO-TPP)Ru=CPh_2] (**1i**)[a]	8.45 (s)		316.30	398 (5.06), 424 (4.97), 532 (4.24)	[12]
[(F_{20}-TPP)Ru=CPh_2] (**1j**)[a]	8.32 (s)		328.70	385 (4.90), 425 (4.89), 526 (4.11), 550 (sh, 4.10), 613(3.13)	[13]
[(2,6-Cl-TPP)Ru=C(Ph)CO_2Et] (**2a**)[a]	8.27 (s)		298.50	397 (5.03), 427 (sh, 4.72), 538 (4.08), 571 (sh, 3.92)	[12]
[(TMP)Ru=C(Ph)CO_2Et] (**2b**)[a]	8.23 (s)		287.50	399 (5.12), 434 (sh, 4.64), 538 (4.03), 576 (sh, 3.78)	[12]
[(F_{20}-TPP)Ru=C(C_6H_4Me-4)$_2$] (**3a**)[a]	8.29 (s)		333.00	385 (4.85), 426 (4.84), 525 (4.10), 550 (4.08)	[12]
[(F_{20}-TPP)Ru=C(C_6H_4OMe-4)$_2$] (**3b**)[a]	8.27 (s)		324.76	386 (4.84), 424 (4.75), 526 (4.11), 547 (4.09)	[12]
[(F_{20}-TPP)Ru=C(C_6H_4Cl-4)$_2$] (**3c**)[a]	8.37 (s)		322.65	386 (4.92), 424 (4.84), 527 (4.10), 552 (4.08)	[12]
[(F_{20}-TPP)Ru=C(C_6H_4OMe-4)CO_2Me] (**4a**)[a]	8.44 (s)		298.85	390 (5.00), 415 (sh, 4.78), 529 (4.19), 550 (sh, 4.15)	[12]
[(F_{20}-TPP)Ru=C($C_6H_4NO_2$-4)CO_2Me] (**4b**)[a]	8.51 (s)		299.44	395 (5.06), 426 (sh, 4.62), 533 (4.05), 562 (sh, 3.93)	[12]
[(F_{20}-TPP)Ru=C(CO_2Me)$_2$] (**5**)[a]	8.57 (s)		280.49	396 (4.98), 429 (sh, 4.48), 535 (3.97), 565 (3.82)	[12]
[(F_{20}-TPP)Ru=C(CH=CHPh)CO_2CH_2(CH=CH)$_2$Me] (**6**)[a]	8.45 (s)		288.71	401 (5.10), 463 (4.17), 530 (4.15)	[12]
[(MeOH)(F_{20}-TPP)Ru=CPh_2] (**7a**)[a]	8.24 (s)		329.00	385 (4.84), 425 (4.83), 525 (4.06), 550 (4.04)	[12]
[(EtSH)(F_{20}-TPP)Ru=CPh_2] (**7b**)[a]	8.29 (s)		330.85	385 (4.90), 425 (4.90), 525 (4.12), 550 (4.10)	[12]
[(Et_2S)(F_{20}-TPP)Ru=CPh_2] (**7c**)[a]	8.26 (s)		338.34	385 (4.89), 424 (4.89), 526 (4.12), 549 (4.10)	[12]
[(MeIm)(F_{20}-TPP)Ru=CPh_2] (**7d**)[a]	8.13 (s)		332.13	398 (4.94), 428 (4.88), 528 (4.20), 551 (sh, 4.05)	[12]
[(py)(F_{20}-TPP)Ru=CPh_2] (**7e**)[a]	8.18 (s)		346.69	390 (4.87), 425 (4.86), 527 (4.01), 550 (sh, 3.92)	[12]
[(Ph_3PO)(F_{20}-TPP)Ru=CPh_2] (**7f**)[a]	8.30 (s)		330.15	385 (4.92), 425 (4.92), 526 (4.13), 549 (4.12)	[12]
[(MeOH)(F_{20}-TPP)Ru=C(Ph)CO_2CH_2CH=CH_2] (**8**)[a]	8.53 (s)		304.34	389 (4.99), 422 (sh, 4.77), 530 (4.12), 555 (sh, 4.05)	[12]
[(MeOH)(F_{20}-TPP)Ru=C(Ph)CO_2Et] (**9**)[a]	8.46 (s)		305.52	388 (4.99), 419 (sh, 4.88), 529 (4.35), 556 (sh, 4.32)	[12]
[(MeOH)(F_{20}-TPP)Ru=C(Ph)CO_2Me] (**10**)[a]	8.46 (s)		304.13	390 (4.97), 420 (sh, 4.78), 530 (4.10), 553 (sh, 4.04)	[12]
[(TPP)Ru=CHP(O)(O^iPr)$_2$][a]	8.6 (s)	15.2 (d)	290	406 (Soret)	[14]
[(TMP)Ru=CHP(O)(O^iPr)$_2$][a]	8.3 (s)	15.3 (d)	285	405 (Soret)	[14]
[(F_{20}-TPP)Ru=CHP(O)(O^iPr)$_2$][a]	8.4 (s)	15.8 (d)		400 (Soret)	[14]
[(TTP)Os=CH(Mes)][b]	8.19	20.78	248	418 (Soret), 518, 550	[5i]
[(TTP)Os=C$HCO_2CH_2CH_2CH_3$][b]	8.36	21.82		408 (Soret)	[5i]
[(TTP)Os=CH(C_6H_4Me-4)][b]	8.21	19.85			[5i]
[(TTP)Os=CH(C_6H_4Et-4)][b]	8.21	19.93			[5i]
[(TTP)Os=CMePh][b]	8.16		263.9	410 (Soret), 424 (sh), 516, 540	[5i]
[(TTP)Os=C(CO_2Et){C(O)CH_2CH_2CH=CH_2}][b]	8.40			398 (Soret), 420 (sh), 432 (sh), 518, 572	[5i]
[(MeIm)(F_{20}-TPP)Os=CPh_2] (**11a**)[a]	7.44 (s)		289.27	385 (sh, 4.65), 408 (4.86), 519 (4.13), 546 (4.12)	[12]

Table 1 (*Continued*)

Complex	^{1}H NMR (δ (ppm))		^{13}C NMR (δ (ppm)) M=*C*	UV–vis (λ_{max} (nm)) (log ε)	Ref.
	H_β	M=C*H*–			
[(py)(TTP)Os=CPh_2] (**11b**)[a]	7.76 (s)		279.16	398 (Soret), 429 (sh), 523, 551	[15]
[{(TPP)Os=CPh_2}$_2$(μ-O)] (**12a**)[a]	8.12 (s)		268.84	408 (5.10), 529 (4.20), 607 (3.95), 735 (3.95)	[15]
[{(TTP)Os=CPh_2}$_2$(μ-O)] (**12b**)[a]	8.08 (s)		266.20	413 (5.12), 532 (4.22), 613 (3.96), 734 (3.97)	[15]
[{(4-F-TPP)Os=CPh_2}$_2$(μ-O)] (**12c**)[a]	8.06 (s)		269.28	409 (5.12), 530 (4.24), 605 (sh, 3.96), 734 (3.98)	[15]
[{(4-Cl-TPP)Os=CPh_2}$_2$(μ-O)] (**12d**)[a]	8.06 (s)		269.94	413 (5.06), 530 (4.14), 606 (sh, 3.88), 735 (3.86)	[15]
[{(4-Br-TPP)Os=CPh_2}$_2$(μ-O)] (**12e**)[a]	8.05 (s)		270.06	413 (5.16), 527 (4.25), 604 (sh, 3.99), 732 (3.91)	[15]
[{(OEP)Os=CPh_2}$_2$(μ-O)][a]				372 (5.03)	[17]
[(F_{20}-TPP)Fe=CPh_2] (**13a**)[a]	8.31 (s)		358.98	404 (5.07), 524 (4.00), 557 (4.14)	[18]
[(F_{20}-TPP)Fe=C(Ph)CO_2Et] (**13b**)[a]	8.56 (s)		327.47	402 (5.11), 521 (4.02), 555 (4.12)	[18]
[(F_{20}-TPP)Fe=C$Ph$$CO_2CH_2CH$=$CH_2$] (**13c**)[a]	8.55 (s)		325.67	402 (5.03), 521 (3.91), 555 (4.01)	[18]
[(MeIm)(F_{20}-TPP)Fe=CPh_2] (**14**)[a]	8.23 (s)		385.44	403 (5.24), 524 (4.20), 557 (4.29)	[18]
[(H_2O)(TPP)Fe=CCl_2][a]	8.77 (s)		224.7		[19a]
[(TTP)Fe=CH($C_6H_3Me_3$-2,4,6)][b]	8.72 (s)	19.71 (s)			[20]
[(TTP)Fe=C$HSiMe_3$][b]	8.69 (s)	24.86 (s)			[20]
[(MeIm)(2,4-Cl-salen)Ru=CPh_2] (**15a**)[c]			317.3	338 (5.71), 400 (5.76), 435 (sh, 5.68)	[21]
[(MeIm)(2,4-Br-salen)Ru=CPh_2] (**15b**)[c]			317.0	338 (5.78), 401 (5.85), 435 (sh, 5.78)	[21]
[(MeIm)(2,4-I-salen)Ru=CPh_2] (**15c**)[c]			316.3	345 (5.87), 405 (5.98), 437 (sh, 5.88)	[21]
[(py)(2,4-Br-salen)Ru=CPh_2] (**15d**)[c]				337 (4.12), 400(4.18), 436 (sh, 4.09)	[21]
[(MeIm)(2,4-Br-salen)Ru=C(C_6H_4OMe-4)$_2$] (**15e**)[c]			317.3	349 (4.22), 417 (4.22), 451 (sh, 4.18)	[21]
[(tpy)(bpy)Ru=C(OMe)CH_2(C_6H_4OMe-4)](ClO_4)$_2$ (**16a**)[d]			317.7	230 (4.47), 285 (4.63), 310 (4.53), 335 (sh, 4.21), 415 (3.94), 515 (sh, 3.22)	[22]
[(tpy)(bpy)Ru=C(OMe)$CH_2{}^t$Bu](ClO_4)$_2$ (**16b**)[d]			328.9	242 (4.56), 285 (4.80), 312 (sh, 4.68), 334 (sh, 4.46), 408 (4.13), 503 (sh, 3.55)	[22]

The spectroscopic data of related iron porphyrin carbene complexes are included for comparison.

[a] In $CDCl_3$ (NMR) or CH_2Cl_2 (UV–vis).

[b] In C_6D_6 (NMR) or C_6H_6 (UV–vis).

[c] In C_6D_5N (NMR) or DMSO (UV–vis).

[d] In CD_2Cl_2 (NMR) or CH_2Cl_2 (UV–vis).

ruthenium carbene complexes [12]. For [(F_{20}-TPP)Ru=CRR′] (**1j**, **3a**–**c**, **4a**, **b**, **5** and **6**), the H_β chemical shifts decrease along the CRR′ order:

$$C(CO_2Me)_2 > C(C_6H_4NO_2\text{-}4)CO_2Me > C(CH{=}CHPh)CO_2CH_2(CH{=}CH)_2Me,$$

$$C(C_6H_4OMe\text{-}4)CO_2Me > C(C_6H_4Cl\text{-}4)_2 > CPh_2 > C(C_6H_4Me\text{-}4)_2, C(C_6H_4OMe\text{-}4)_2$$

indicating a decrease in H_β chemical shift with decreasing electron-withdrawing strength of the carbene groups. The M=*C* chemical shifts of [(Por)Ru=CPh_2] (**1a**–**j**) in the ^{13}C NMR spectra follow a porphyrin ligand order:

$$F_{20}\text{-TPP} > 2,6\text{-Cl-TPP} > 4\text{-Br-TPP}, 4\text{-Cl-TPP}, 4\text{-MeO-TPP} > 4\text{-F-TPP} > TMP > TPP > TTP, 3,4,5\text{-MeO-TPP}$$

which reveals that a more electron-withdrawing porphyrin ligand generally results in larger chemical shifts of the M=*C* signals. In the cases of [(F_{20}-TPP)Ru=CPh_2] (**1j**) and [(L)(F_{20}-TPP)Ru=CPh_2] (**7a**–**e**), the H_β chemical shifts of the latter are smaller than that of the former and become smaller along the L order:

$$EtSH, Et_2S, MeOH > py > MeIm$$

This shows that coordination of L to **1j** leads to an upfield shift of the H_β signal, with MeIm exhibiting the largest trans influence.

A direct comparison among the spectroscopic features of ruthenium, osmium and iron carbene complexes has been made from [(MeIm)(F_{20}-TPP)M=CPh_2] (M = Fe, **14**; Ru, **7d**; Os, **11a**) [12], whose H_β and M=*C* chemical shifts both decrease along the order:

$$Fe > Ru > Os$$

Such an order is different from the Pauling electronegativity trend of Fe < Ru = Os. A rationalization for this phenomenon is given on the basis of a competition among the inductive effect, M → Por back bonding and porphyrin ring current effect [12].

Salen-supported ruthenium carbene complexes [(L)(salen)Ru=CR_2] (**15a**–**e**) have Ru=*C* chemical shifts of δ 316.3–317.3 ppm, which are within the foregoing range

observed for the porphyrin-supported ruthenium carbene complexes. The UV–vis absorption spectra of **15a–e** show intense bands at $\lambda_{max} \approx 340$ and 405 nm ($\log \varepsilon > 4$), the former should originate from intraligand charge-transfer transitions of the coordinated salen ligands. A weak low energy band appearing at $\lambda_{max} \approx 630$–660 nm ($\log \varepsilon = 2.80$–$3.12\ dm^3\ mol^{-1}\ cm^{-1}$) in the spectra of **15b** and **15d** is attributed to d–d transitions [21].

Complex [(tpy)(bpy)Ru=C(OMe)CH_2(C_6H_4OMe-4)]$(ClO_4)_2$ (**16a**) bearing polypyridine ligands has a M=*C* chemical shift of δ 317.7 ppm [22], very similar to those of the ruthenium salen carbene complexes **15a–e**. Changing the carbene group in **16a** to C(OMe)$CH_2{}^t$Bu increases the M=*C* chemical shift to δ 328.9 ppm (**16b**). In the UV–vis absorption spectra of **16a** and **16b**, intense intraligand $\pi \rightarrow \pi^*$ transition bands appear at $\lambda_{max} \leq 350$ nm ($\varepsilon_{max} \geq 10^4\ dm^3\ mol^{-1}\ cm^{-1}$); $d_\pi(Ru^{II}) \rightarrow \pi^*$(polypyridine) MLCT transitions are observed as a moderately intense band at $\lambda_{max} \approx 410$ nm ($\varepsilon_{max} = (8$–$10) \times 10^3\ dm^3\ mol^{-1}\ cm^{-1}$) [22].

Following our observation of an emissive metal $\rightarrow \pi^*$(carbene) CT excited state in solution at room temperature by using a hexanuclear platinum(II) macrocycle containing chelating bis-carbene ligands [23], and the report of rhenium(I) *N*-heterocyclic carbene complexes that are emissive at room temperature and 77 K [24], we found that the polypyridine-supported ruthenium carbene complexes **16a** and **16b** produce red emission with λ_{max} 597 and 615 nm, respectively, upon excitation at λ 415 nm in *n*-butyronitrile glass at 77 K [22]. The emission bands shift to 616 and 630 nm at 77 K and 649 and 711 nm at 298 K, respectively, when measured in the solid state [22]. These emissions are tentatively attributed to $d_\pi(Ru^{II}) \rightarrow \pi^*$(polypyridine) ^{3}MLCT in nature.

2.3. Structure

Since the publication of the previous review [9], about 20 additional ruthenium and osmium porphyrin carbene complexes have been structurally characterized by X-ray crystal analysis, including **1g** and **1i**, **3b**, **7a**, **7b**, **7d** and **7f**, **8–10**, **11a** [12], **1j** [13], **11b**, **12b** [15], [(TTP)Ru=C($C_6H_4CF_3$-3)$_2$] [25], [(MeOH)(TTP)Ru=CPh_2] [26], [(py)(TTP)Ru=CR_2] (R = C($C_6H_4CF_3$-3), C(COPh)$_2$) [27] and [{(OEP)Os=CPh_2}$_2$(μ-O)] [17]. The M=C bond distances and R–C–R′ angles in these M=CRR′ complexes along with those in structurally characterized iron porphyrin carbene complexes **13a**, **14** [18] and [(H_2O)(TPP)Fe=CCl_2] [19b], ruthenium salen carbene complexes **15a–e** [21] and polypyridine-supported ruthenium carbene complex **16a** [22], are summarized in Table 2. Also included in this table are related metal carbene complexes [(tmtaa)Fe=CPh_2] (H_2tmtaa = tetramethyldibenzotetraazaannulene) [28],

Table 2
Selected bond distances and angles of ruthenium, osmium and iron carbene complexes

Complex	M=C (Å)	R–C–R′ (°)	Ref.
[(2,6-Cl-TPP)Ru=CPh_2] (**1g**)	1.859(5)	110.6(4)	[12]
[(3,4,5-MeO-TPP)Ru=CPh_2] (**1i**)	1.866(7)	114.7(6)	[12]
[(F_{20}-TPP)Ru=CPh_2] (**1j**)	1.842(4)	113.4(3)	[13]
[(F_{20}-TPP)Ru=C(C_6H_4OMe-4)$_2$] (**3b**)	1.854(4)	111.5(4)	[12]
[(TTP)Ru=C($C_6H_4CF_3$-3)$_2$]	1.841(6)	116.1(5)	[25]
[(MeOH)(F_{20}-TPP)Ru=CPh_2] (**7a**)	1.853(3)	112.9(3)	[12]
[(MeOH)(TTP)Ru=CPh_2]	1.845(3)	112.2(3)	[26]
[(EtSH)(F_{20}-TPP)Ru=CPh_2] (**7b**)	1.858(5)	114.2(4)	[12]
[(MeIm)(F_{20}-TPP)Ru=CPh_2)] (**7d**)	1.876(3)	113.1(2)	[12]
[(Ph_3PO)(F_{20}-TPP)Ru=CPh_2)] (**7f**)	1.853(3)	110.6(2)	[12]
[(MeOH)(F_{20}-TPP)Ru=C(Ph)CO_2CH_2CH=CH_2] (**8**)	1.806(3)	108.0(3)	[12]
[(MeOH)(F_{20}-TPP)Ru=C(Ph)CO_2Et] (**9**)	1.868(3)	111.6(3)	[12]
[(MeOH)(F_{20}-TPP)Ru=C(Ph)CO_2Me)] (**10**)	1.850(3)	110.6(2)	[12]
[(py)(TTP)Ru=C($C_6H_4CF_3$-3)$_2$]	1.868(3)	116.8(6)	[27]
[(py)(TTP)Ru=C(COPh)$_2$]	1.877(8)	112.8(2)	[27]
[(MeIm)(F_{20}-TPP)Os=CPh_2] (**11a**)	1.902(3)	112.8(3)	[12]
[(py)(TTP)Os=CPh_2] (**11b**)	1.903(7)	112.4(6)	[15]
[{(TTP)Os=CPh_2}$_2$(μ-O)] (**12b**)	1.910(1)	110.7(3)	[15]
[{(OEP)Os=CPh_2}$_2$(μ-O)]	1.930(8)	114.4(7)	[17]
[(F_{20}-TPP)Fe=CPh_2] (**13a**)	1.767(3)	111.5(3)	[18]
[(MeIm)(F_{20}-TPP)Fe=CPh_2] (**14**)	1.827(5)	111.0(4)	[18]
[(H_2O)(TPP)Fe=CCl_2]	1.83(3)		[19b]
[(MeIm)(2,4-Cl-salen)Ru=CPh_2] (**15a**)	1.913(5)	114.9(6), 116.4(5)	[21]
[(MeIm)(2,4-Br-salen)Ru=CPh_2] (**15b**)	1.921(12)	114(1), 116(1)	[21]
[(MeIm)(2,4-I-salen)Ru=CPh_2] (**15c**)	1.919(14)	113(1), 117(1)	[21]
[(py)(2,4-Br-salen)Ru=CPh_2] (**15d**)	1.917(4)	115.7(3)	[21]
[(MeIm)(2,4-Br-salen)Ru=C(C_6H_4OMe-4)$_2$] (**15e**)	1.910(2)	115(2), 116(2)	[21]
[(tpy)(bpy)Ru=C(OMe)CH_2(C_6H_4OMe-4)]$(ClO_4)_2$ (**16a**)	1.933(6)	117.4(5)	[22]
[(tmtaa)Fe=CPh_2]	1.794(3)	115.7(3)	[28]
[(tmtaa)Ru=CPh_2]	1.874(8)	116.4(6)	[29]
[Cl_2(pybox)Ru=C(CO_2Me)$_2$]	1.880(7)		[30]

[(tmtaa)Ru=CPh$_2$] [29] and [Cl$_2$(pybox)Ru=C(CO$_2$Me)$_2$] (pybox = 2,6-bis(4(*S*)-isopropyloxazolin-2-yl)pyridine) [30].

The ruthenium porphyrin carbene complexes in Table 2 have Ru=C distances of 1.806(3)–1.877(8) Å and R–C–R′ angles of 108.0(3)–116.8(6)°, comparable to those of previously reported analogues [9]. For the five-coordinate complexes [(Por)Ru=CR$_2$], a shorter Ru=C bond generally corresponds to a more strongly electron-withdrawing carbene or porphyrin ligand, which is ascribed to a stronger Ru → C π-backbonding and a decrease in the electron density of the ruthenium ion, respectively (the latter increases electron donation from the carbene ligand) [12]. Conversion of [(Por)Ru=CR$_2$] to six-coordinate complexes [(L)(Por)Ru=CR$_2$] appreciably lengthens the Ru=C bonds due to trans influence, as shown by comparing the Ru=C distances between **1j** and **7**, or between [(TTP)Ru=C(C$_6$H$_4$CF$_3$-3)$_2$] and [(py)(TTP)Ru=C(C$_6$H$_4$CF$_3$-3)$_2$]. Among the L of MeOH, EtSH, MeIm and Ph$_3$PO, MeIm exhibits the largest trans influence; the coordination of MeIm to **1j** lengthens the Ru=C bond by 0.034 Å.

Six-coordinate osmium porphyrin carbene complexes **11a** and **11b** show almost identical Os=C distances of 1.902(3) and 1.903(7) Å and R–C–R′ angles of 112.8(3)° and 112.4(6)°, respectively. The Os=C bonds are considerably longer than, where the R–C–R′ angles are comparable to, those of the ruthenium analogues.

The structure determination of [(MeIm)(F$_{20}$-TPP)M=CPh$_2$] (M = Fe, **14**; Ru, **7d**; Os, **11a**) (Fig. 6) allows a direct comparison of the structural features among iron, ruthenium and osmium porphyrin carbene complexes [12]. The M=C distances in [(MeIm)(F$_{20}$-TPP)M=CPh$_2$] (Fe, 1.827(5) Å; Ru, 1.876(3) Å; Os, 1.902(3) Å) follow the order of

$$Fe < Ru < Os$$

This order of M=C distances is opposite to the order of the H$_\beta$ and M=*C* chemical shifts found for the same complexes (see above). Other notable differences in the structures of the iron, ruthenium, and osmium carbene complexes are the substantial distortion of the porphyrin ring in the iron complex **14** and the considerably bent M-MeIm moieties in the ruthenium and osmium complexes **7d** and **11a** [12]. In addition, the lengthening of Fe=C distance by 0.06 Å on going from [(F$_{20}$-TPP)Fe=CPh$_2$] (**13a**) to [(MeIm)(F$_{20}$-TPP)Fe=CPh$_2$] (**14**) [18] reflects a larger trans influence of MeIm in iron carbene complex compared to that in the ruthenium counterpart.

Interestingly, in the crystal structure of [(F$_{20}$-TPP)Ru=C(C$_6$H$_4$OMe-4)$_2$] (**3b**) [12], the carbene complex exists as a one-dimensional coordination polymer (Fig. 7) wherein each of the bis(*p*-methoxyphenyl)carbene ligand links two ruthenium atoms through the carbene carbon atom and one of the two methoxy oxygen atoms. Such a bridging carbene ligand has not been observed in the crystal structures of other metalloporphyrin carbene complexes.

For the oxo-bridged osmium porphyrin carbene complex **12b** (Fig. 8), its Os=C distance is 1.910(1) Å, similar to those in **11a** and **11b**. The two TTP rings in the dinuclear oxo-bridged complex adopt an orientation in between the fully staggered and eclipsed conformations. Replacing the TTP ligand with a more electron-rich OEP ligand increases the Os=C distance to 1.930(8) Å [17]. Both **12b** and [{(OEP)Os=CPh$_2$}$_2$(μ-O)] have a linear axial C=Os–O–Os=C moiety with an Os–O–Os angle of ∼179°, coupled with nearly coplanar axial Ph–C–Ph carbene planes with small dihedral angles of ∼4.5° for **12b** and 10.1° for [{(OEP)Os=CPh$_2$}$_2$(μ-O)]. These structural features suggest the presence of delocalized C–Os–O–Os–C and Os–O–Os π-bonding in the molecules [15], which may be a cause for the diamagnetism of [{(Por)Os=CPh$_2$}$_2$(μ-O)].

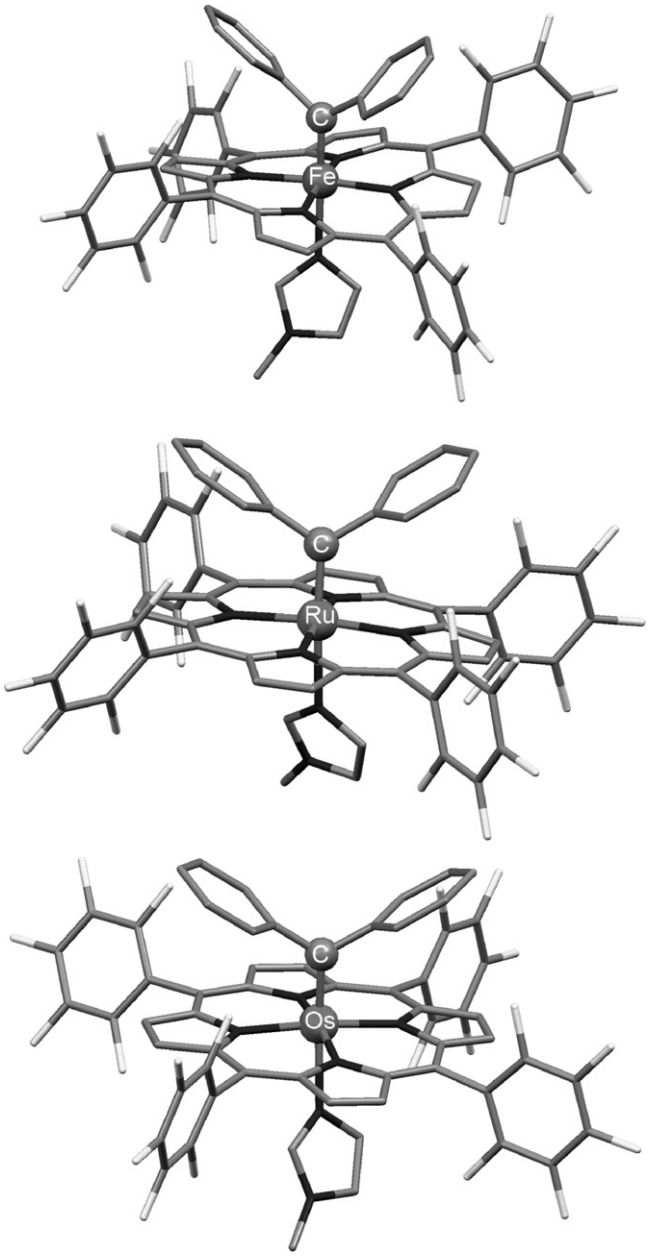

Fig. 6. Structures of [(MeIm)(F$_{20}$-TPP)M=CPh$_2$] (M = Fe, **14**; Ru, **7d**; Os, **11a**) [12].

Ruthenium salen carbene complexes **15a–e** have been characterized by X-ray crystal analysis [21]. These ruthenium carbene complexes show markedly long Ru=C distances of 1.910(2)–1.921(12) Å compared to the ruthenium porphyrin analogues, with the R–C–R′ angles being 113(1)–117(1)°. The

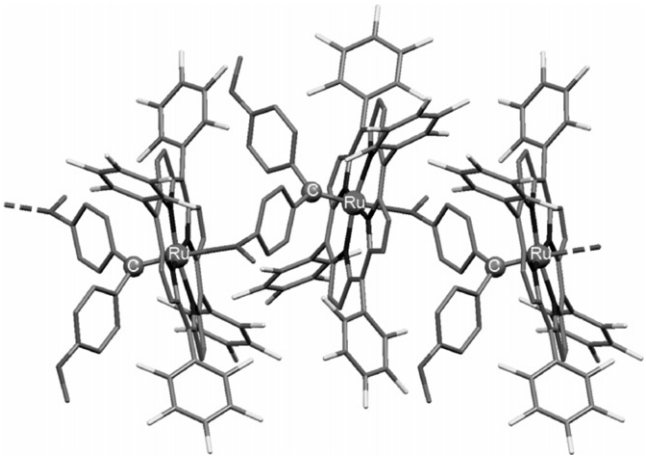

Fig. 7. Structure of [(F_{20}-TPP)Ru=C(C_6H_4OMe-4)$_2$] (**3b**) [12] showing a one-dimensional polymer chain.

structures of **15b**, **15d** and **15e** are depicted in Fig. 9. Note that **15e** contains the same carbene ligand as **3b**; however, unlike the latter, the former does not exist as a one-dimensional coordination polymer in the solid state, apparently due to the lack of vacant coordination site for the formation of a carbene bridge.

Polypyridine-supported ruthenium carbene complex **16a** (Fig. 10) exhibits a Ru=C distance of 1.933(6) Å and an R–C–R′ angle of 117.4(5)°; the Ru=C distance is even longer than those in the ruthenium salen carbene complexes.

From the structural data listed in Table 2, it is evident that ruthenium carbene complexes supported by porphyrin ligands have Ru=C distances comparable to those of the complexes supported by tmtaa or pybox ligands. Similarly, the Fe=C distances in iron porphyrin carbene complexes are also comparable to that of their tmtaa counterpart. However, replacing the porphyrin ligands with salens or polypyridines significantly lengthens the Ru=C bonds.

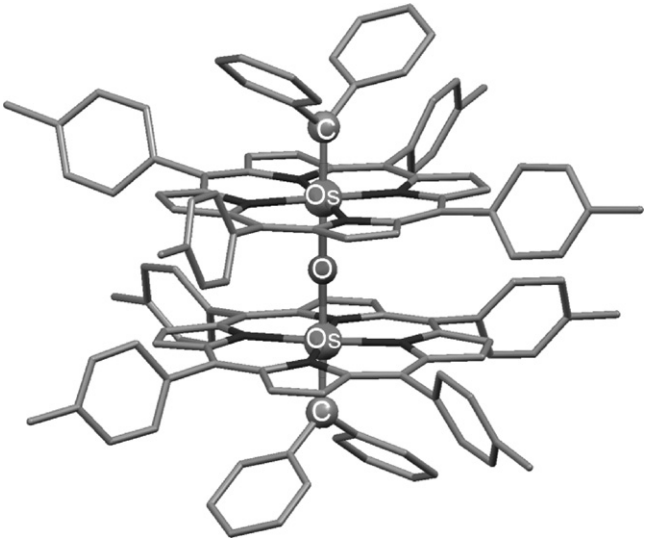

Fig. 8. Structure of [{(TTP)Os=CPh_2}$_2$(μ-O)] (**12b**) [15].

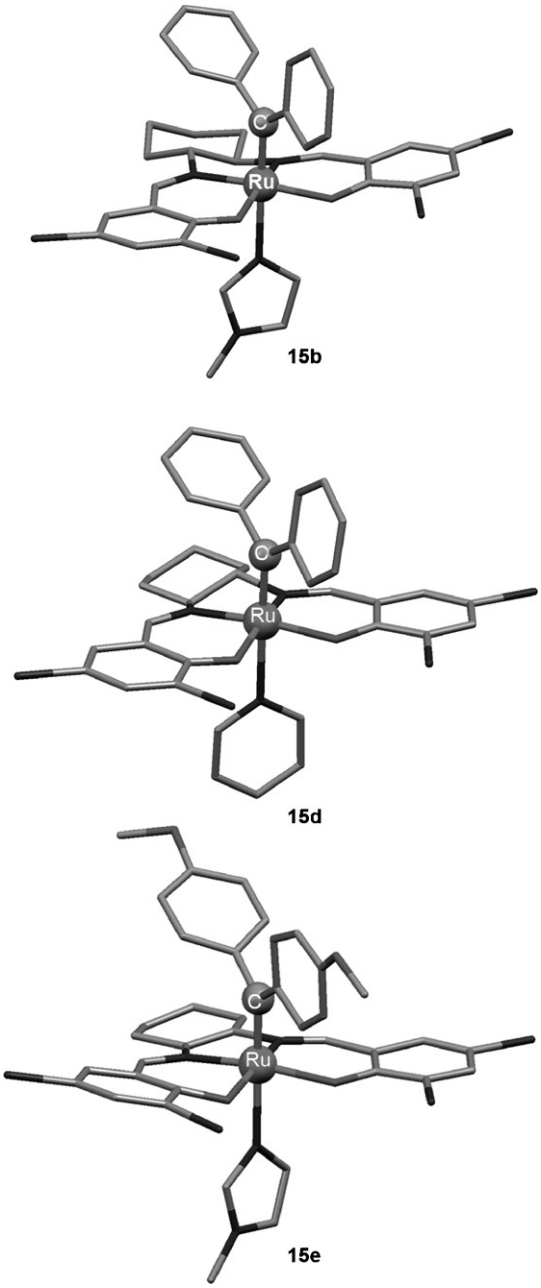

Fig. 9. Structures of [(L)(2,4-Br-salen)Ru=CPh_2] (L = MeIm, **15b**; py, **15d**) and [(MeIm)(2,4-Br-salen)Ru=C(C_6H_4OMe-4)$_2$] (**15e**) [21].

2.4. Electrochemistry

The first electrochemical studies on ruthenium and osmium porphyrin carbene complexes appeared in 2004 [12], in which we extensively examined the redox behavior of 19 ruthenium porphyrin carbene complexes **1c–j**, **2a**, **2b**, **3a**, **3c**, **4a**, **4b**, **7b–d**, **8** and **10**, together with osmium porphyrin carbene complex **11a**, by cyclic voltammetry. The redox behavior of iron porphyrin carbene complexes **13a** and **14** was also examined for comparison. Listed in Table 3 are the half-wave potentials (versus $Cp_2Fe^{+/0}$) observed for these metalloporphyrin carbene complexes. Fig. 11 shows the cyclic voltammograms of **1c**, **1f**, **7d** and **11a**.

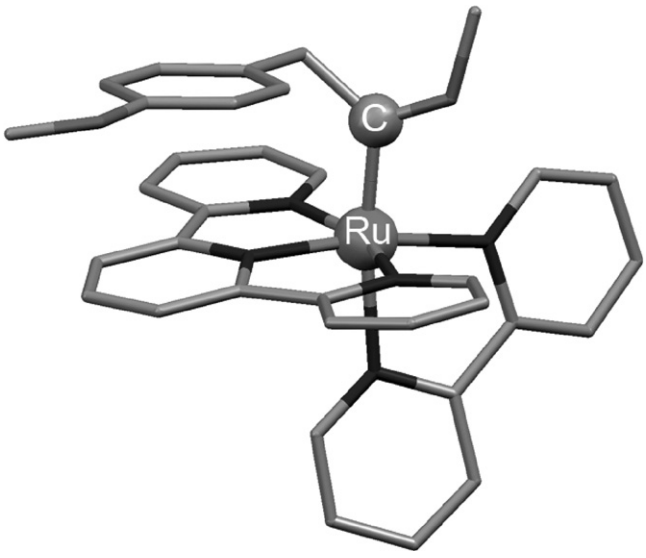

Fig. 10. Structure of [(tpy)(bpy)Ru=C(OMe)CH_2(C_6H_4OMe-4)](ClO_4)$_2$ (**16a**) with omission of the counter-anions [22].

The carbene complexes supported by F_{20}-TPP and 2,6-Cl-TPP ligands almost all show one reversible oxidation couple ($E_{1/2}$ 0.13–0.77 V). [(MeIm)(F_{20}-TPP)Os=CPh_2] (**11a**) and the carbene complexes containing the other porphyrin ligands exhibit two reversible oxidation couples ($E_{1/2}$ 0.06–0.32 and 0.81–1.07 V), except for [(4-MeO-TPP)Ru=CPh_2] (**1c**), which shows three reversible oxidation couples ($E_{1/2}$ 0.20, 0.80 and 1.03 V). For nearly all the carbene complexes supported by F_{20}-TPP ligand, a reversible reduction couple is observed ($E_{1/2}$ −1.25 to −1.73 V). The reduction couples for the carbene complexes bearing other porphyrin ligands are not clearly observable (though partially observed in some cases), probably due to overlap with the reduction of the solvent.

Table 3
Half-wave potentials (V vs. $Cp_2Fe^{+/0}$) of iron, ruthenium and osmium porphyrin carbene complexes [12]

Complex	E_{O1}	E_{O2}	E_{R1}
[(4-MeO-TPP)Ru=CPh_2] (**1c**)	0.20	0.80[a]	
[(4-F-TPP)Ru=CPh_2] (**1d**)	0.26	0.94	
[(4-Cl-TPP)Ru=CPh_2] (**1e**)	0.32	0.96	−1.88[b]
[(4-Br-TPP)Ru=CPh_2] (**1f**)	0.30	0.96	−1.89[b]
[(2,6-Cl-TPP)Ru=CPh_2] (**1g**)	0.32		−1.88[b]
[(TMP)Ru=CPh_2] (**1h**)	0.19	0.98	
[(3,4,5-MeO-TPP)Ru=CPh_2] (**1i**)	0.25	0.81	
[(F_{20}-TPP)Ru=CPh_2] (**1j**)	0.46		−1.53
[(2,6-Cl-TPP)Ru=C(Ph)CO_2Et] (**2a**)	0.42		−1.73
[(TMP)Ru=C(Ph)CO_2Et] (**2b**)	0.32	0.92	
[(F_{20}-TPP)Ru=C(C_6H_4Me-4)$_2$] (**3a**)	0.44		−1.55
[(F_{20}-TPP)Ru=C(C_6H_4Cl-4)$_2$] (**3c**)	0.57		−1.50
[(F_{20}-TPP)Ru=C(C_6H_4OMe-4)CO_2Me] (**4a**)	0.50		−1.51
[(F_{20}-TPP)Ru=C($C_6H_4NO_2$-4)CO_2Me] (**4b**)	0.77		−1.25
[(EtSH)(F_{20}-TPP)Ru=CPh_2] (**7b**)	0.52		−1.53
[(Et_2S)(F_{20}-TPP)Ru=CPh_2] (**7c**)	0.52		−1.53
[(MeIm)(F_{20}-TPP)Ru=CPh_2] (**7d**)	0.33		−1.63
[(MeOH)(F_{20}-TPP)Ru=C(Ph)CO_2CH_2 CH=CH_2] (**8**)	0.63		−1.46
[(MeOH)(F_{20}-TPP)Ru=C(Ph)CO_2Me] (**10**)	0.65		−1.47
[(MeIm)(F_{20}-TPP)Os=CPh_2] (**11a**)	0.06	1.07	−1.71
[(F_{20}-TPP)Fe=CPh_2] (**13a**)	0.35		−1.52
[(MeIm)(F_{20}-TPP)Fe=CPh_2] (**14**)	0.13		−1.67

[a] E_{O3} = 1.03 V.
[b] $E_{p,c}$.

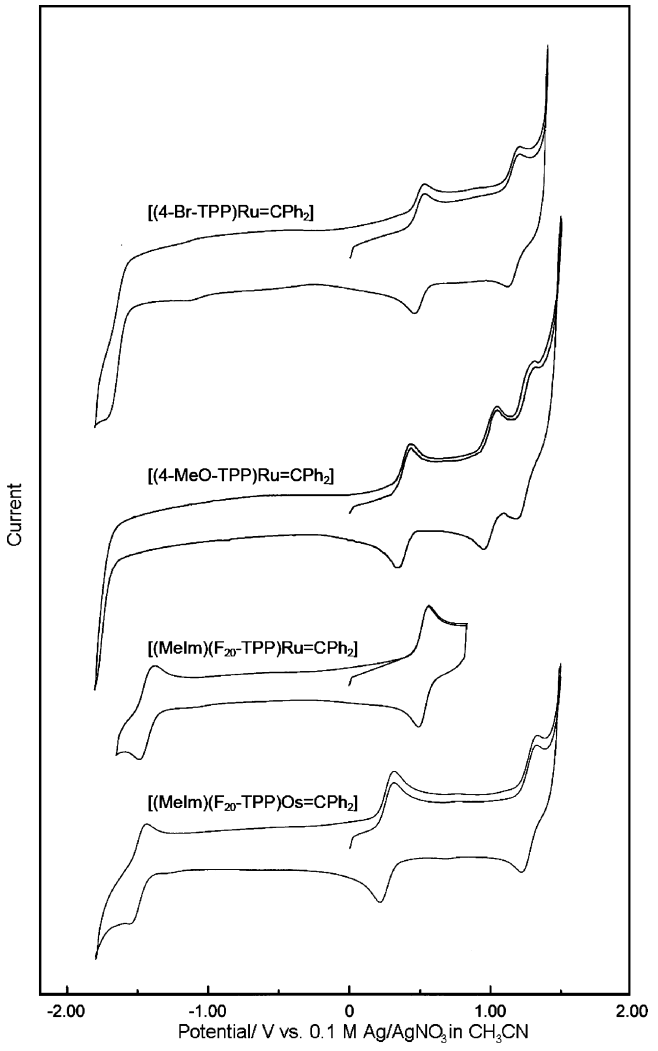

Fig. 11. Cyclic voltammograms of [(Por)Ru=CPh_2] (Por = 4-MeO-TPP, **1c**;4-Br-TPP, **1f**) and [(MeIm)(F_{20}-TPP)M=CPh_2] (M = Ru, **7d**; Os, **11a**) [12] in CH_2Cl_2 with 0.1 M $^nBu_4NPF_6$ as supporting electrolyte. Conditions: working electrode, glassy carbon; scan rate, 100 mV s^{-1}.

Spectroelectrochemistry of **1d**, **1h** and **2a**, **2b** in CH_2Cl_2 [12] reveals collapse of the two Soret bands ($\lambda_{max} \approx 395$ and 430 nm) of the diphenylcarbene complex **1d** or **1h** into a single band ($\lambda_{max} \approx 410$ nm) and a red shift (λ_{max} from ∼398 to ∼410 nm) of the single Soret band of the phenyl(ethoxycarbonyl)carbene complex **2a** or **2b** upon electrolysis at a potential in between the $E_{1/2}$ of the corresponding first and second oxidation couples. This indicates a smaller effect of carbene substituents on the electronic spectra of the oxidized ruthenium porphyrin carbene species. As the UV–vis absorption spectra recorded at different time intervals showed no prominent bands in the 600–800 nm region, the porphyrin ring should not be oxidized in the course of the electrolysis.

On the basis of the spectroelectrochemical studies, the first oxidation of ruthenium porphyrin carbene complexes (except **4b** with an $E_{1/2}$ value comparable to that for porphyrin ring oxidation) is attributed to a metal-centered process [12]. A similar assignment can be made to the first oxidation of the iron and osmium analogues **11a**, **13a** and **14** in view of their $E_{1/2}$ values. Other redox couples of the ruthenium, osmium and iron porphyrin carbene complexes are assigned to originate from porphyrin-centered processes.

The $E_{1/2}$ value for the first oxidation of ruthenium porphyrin carbene complexes decreases with increasing electron-donating strength of the carbene, porphyrin, or trans ligands. This is consistent with the effects of carbene substituents, porphyrin substituents, or trans ligands on the H_β and/or M=*C* chemical shifts of these complexes [12]. For the first oxidation of [(MeIm)(F_{20}-TPP)M=CPh_2] (**7d**, **11a**, **14**), the $E_{1/2}$ value decreases along the order

Ru > Fe > Os

which is different from the order of their H_β and M=*C* chemical shifts but similar to the order of $E_{1/2}$ values observed for bis-pyridine metalloporphyrins [(OEP)M($py)_2$] ($E_{1/2}$ = −0.15 (Fe), −0.02 (Ru), −0.37 V (Os)) [31].

Ruthenium salen carbene complexes **15a–e** exhibit a series of irreversible or quasi-reversible oxidation waves, whose potentials are listed in Table 4 [21]. The first oxidation wave is irreversible and occurs at a potential of $E_{p,a}$ −0.04 to 0.15 V, which is assigned to the metal-centered process. These potentials are less anodic than those for the metal-centered oxidation of ruthenium porphyrin carbene complexes, indicating that the ruthenium atoms in the salen complexes **15a–e** are easier to be oxidized. The quasi-reversible waves ($E_{1/2}$ 0.86–1.28 V) of **15a–e** could originate from ligand-centered oxidations.

Three reversible/quasi-reversible couples appear in the cyclic voltammograms of polypyridine-supported ruthenium carbene complexes **16a** ($E_{1/2}$ = −2.03, −1.57, 0.99 V) and **16b** ($E_{1/2}$ = −2.04, −1.50, 1.00 V) [22], as shown from the cyclic voltammogram of **16a** in Fig. 12. The oxidation couple with $E_{1/2} \approx 1.0$ V is attributed to the metal-centered process, which occurs at a markedly more anodic potential than the corresponding oxidation of ruthenium porphyrin carbene complexes, probably due mainly to the dicationic nature of **16a** and **16b**. The other redox couples of **16a** and **16b** are ascribed to the reduction of the polypyridine ligands.

Table 4
Oxidation potentials (V vs. $Cp_2Fe^{+/0}$) of ruthenium carbene complexes supported by salen ligands [21]

Complex	Oxidation potential
[(MeIm)(2,4-Cl-salen)Ru=CPh_2] (**15a**)	0.08[a], 0.24[a], 0.36[a], 0.77[a], 0.86[b], 1.02[b]
[(MeIm)(2,4-Br-salen)Ru=CPh_2] (**15b**)	0.04[a], 0.25[a], 0.36[a], 0.86[b], 1.05[b], 1.25[b]
[(MeIm)(2,4-I-salen)Ru=CPh_2] (**15c**)	0.06[a], 0.25[a], 0.34[a], 0.77[a], 0.98[b], 1.28[b]
[(py)(2,4-Br-salen)Ru=CPh_2] (**15d**)	0.15[a], 0.40[a], 0.63[a], 0.89[b]
[(MeIm)(2,4-Br-salen)Ru=C(C_6H_4OMe-4)$_2$] (**15e**)	−0.04[a], 0.11[a], 0.23[a], 0.71[a], 0.88[b], 1.14[b]

[a] Irreversible, $E_{p,a}$.
[b] Quasi-reversible, $E_{1/2}$.

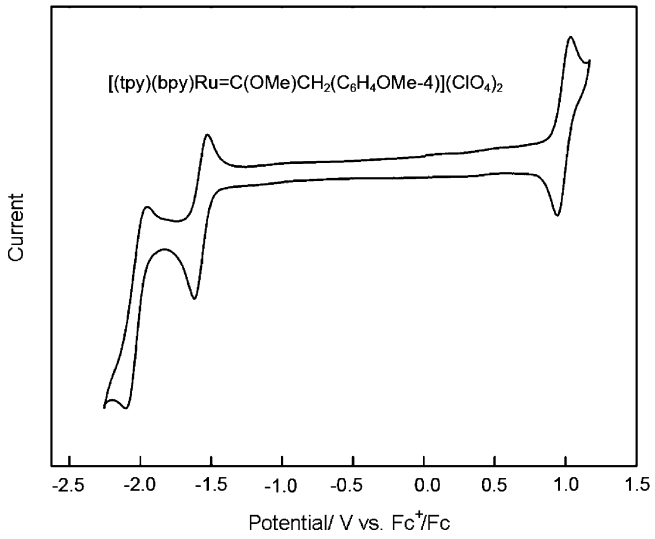

Fig. 12. Cyclic voltammogram of [(tpy)(bpy)Ru=C(OMe)CH_2(C_6H_4OMe-4)]($ClO_4)_2$ (**16a**) in CH_2Cl_2 with 0.1 M $^nBu_4NPF_6$ as supporting electrolyte [22]. Conditions: working electrode, glassy carbon; scan rate, 50 mV s^{-1} (Fc^+/Fc = ferrocenium/ferrocene).

2.5. Reactivity

In the previous review [9], we have described the following reactivities of ruthenium and osmium porphyrin carbene complexes: (i) reaction of [(OEP)Ru=$CHCO_2Et$] with PPh_3 to give [Ru(OEP)PPh_3] and diethyl maleate and fumarate as reported by Collman and co-workers [32], (ii) formation of osmium ylide complexes from the reaction of [(TTP)Os=CHR] (R = CO_2Et, $SiMe_3$) with *para*-substituted pyridines 4-X-C_5H_4N, and reaction of [(TTP)Os=$CHCO_2Et$] with alkenes to afford cyclopropanation products, as reported by Woo and co-workers [5a,33], (iii) cyclopropanation of styrene by [(TPP)Ru=C($CO_2Et)_2$] as reported by Simonneaux and co-workers [34] and (iv) reaction of [(F_{20}-TPP)Os(=$CPh_2)_2$] with alkenes and allylic C–H bonds to form cyclopropanation and C–H insertion products, respectively, as reported by our group [16].

Woo and co-workers subsequently reported that the coordinated carbene ligand in [(TTP)Os=C(CO_2Et){C(O)CH_2-CH_2CH=CH_2}] undergoes intramolecular cyclopropanation to give ethyl 2-oxo[3.1.0]bicyclohexanecarboxylic acid ester upon heating in toluene at 110 °C [5i]. Under a CO atmosphere, the intramolecular cyclopropanation occurs rapidly at 10 °C (reaction 1 in Fig. 13).

We examined the reaction of oxo-bridged osmium porphyrin carbene complexes **12a–e** with styrene at 80 °C and observed no cyclopropanation product even after 30 h [15]. However, **12b** can catalyze the intermolecular cyclopropanation of styrene with N_2CHCO_2Et and intramolecular cyclopropanation of *cis*-pent-2-enyl diazoacetate to afford the corresponding cyclopropanes in 99% (*trans*/*cis* 9.4:1) and 78% yields, respec-

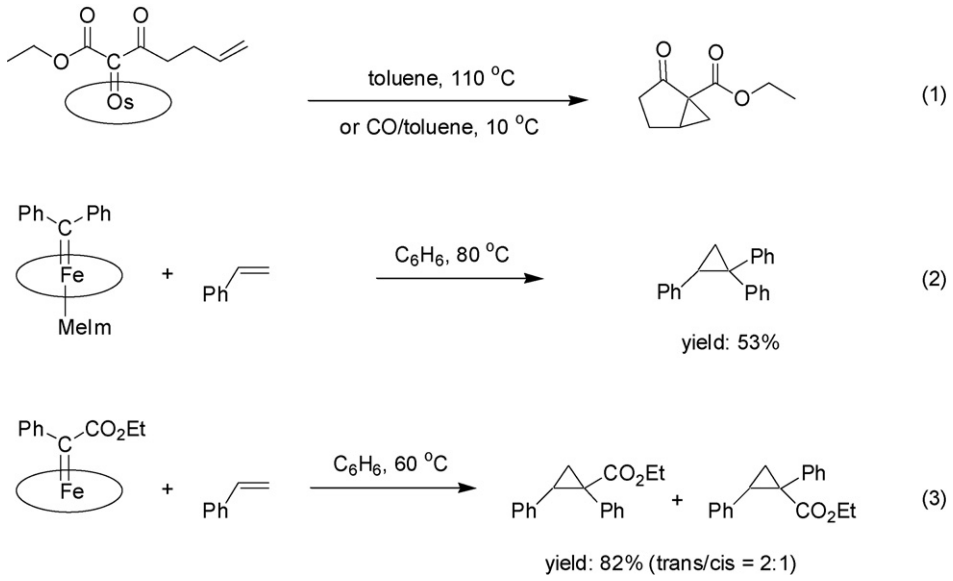

Fig. 13. Reactivity of [(TTP)Os=C(CO_2Et){C(O)CH_2CH_2CH=CH_2}] [5i], [(F_{20}-TPP)Fe=C(Ph)CO_2Et] (**13b**) and [(MeIm)(F_{20}-TPP)Fe=CPh_2] (**14**) [18].

tively. Moreover, this complex is an active catalyst for the C–H insertion reaction between cyclohexene and N_2CHCO_2Et, with the product obtained in 43% yield. The reaction of **12b** with pyridine produces [(py)(TTP)Os=CPh_2] (**11b**), as described above.

Iron porphyrin carbene complex [(F_{20}-TPP)Fe=CPh_2] (**13a**) is unreactive toward stoichiometric cyclopropanation of styrene [18], like previously reported [(Por*)Ru=CPh_2] [35], although both complexes can catalyze intermolecular cyclopropanation reaction between styrenes and N_2CHCO_2Et, and **13a** can catalyze the intramolecular cyclopropanation of allylic diazoacetates. Interestingly, we found that, upon the reaction of MeIm with **13a**, the resultant six-coordinate complex [(MeIm)(F_{20}-TPP)Fe=CPh_2] (**14**) reacts with styrene at 80 °C to afford 1,1,2-triphenylcyclopropane in 53% yield (reaction 2 in Fig. 13) [18]. This could result from the trans effect of MeIm, which weakens the Fe=C bond as evident from the longer Fe=C distance in **14** than in **13a**.

Replacing a phenyl group in the diphenylcarbene ligand of **13a** with a CO_2Et group also activates the coordinated carbene ligand. When we treated [(F_{20}-TPP)Fe=C(Ph)CO_2Et] (**13b**) with excess styrene in benzene at 60 °C for 15 h, 1,2-diphenylcyclopropanecarboxylic acid ethyl ester was obtained in 82% yield (*trans*/*cis* 2.0:1) (reaction 3 in Fig. 13) [18]. Competitive cyclopropanation experiment (*p*-XC_6H_4CH=CH_2 versus styrene) reveals the product ratios of 2.6, 1.6, 1.2 and 0.69 for X = MeO, Me, Cl and CF_3, respectively, which lead to a linear Hammett plot with a small negative ρ value of -0.41 ± 0.05 comparable to that of the cyclopropanation of styrenes with N_2CHCO_2Et catalyzed by [(TTP)Fe] ($\rho = -0.68 \pm 0.07$) [36].

The cyclopropane formation from styrenes and **13b** or **14** is the first alkene cyclopropanation by an isolated iron porphyrin carbene complex without the aid of photolysis. Previously, Suslick and co-workers reported alkene cyclopropanation by iron porphyrin halocarbene complexes upon photolytic cleavage of the iron–carbene bonds [37]. Woo and co-workers reported the

Table 5
Stoichiometric C–H insertion reaction of [(F_{20}-TPP)Fe=C(Ph)CO_2Et] (**13b**) and [(MeIm)(F_{20}-TPP)Fe=CPh_2] (**14**) with alkenes and tetrahydrofuran [18]

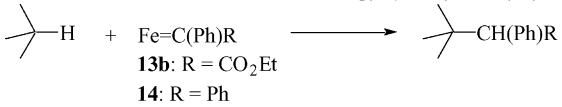

Complex	Alkene	*T* (°C)	Time (h)	Product	Yield (%)
13b	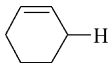	80	24	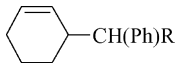	64[a]
14		80	36		24
13b		65	24	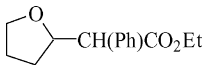	88[b]
13b	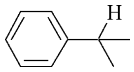	80	15	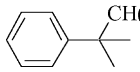	83
13b		60	24		67
13b		25	48		15
14		80	20		59

[a] A mixture of two diastereomers in a molar ratio of 1.2:1.
[b] A mixture of two diastereomers in a molar ratio of 2:1.

formation of cyclopropanes from alkenes and spectroscopically characterized [(TTP)Fe=CHR] (R = 2,4,6-$Me_3C_6H_2$ or $SiMe_3$) [20].

Complexes **13b** and **14** can react with cyclohexene, tetrahydrofuran and cumene, affording the C–H insertion products in up to 64%, 88%, and 83% yield, respectively (Table 5). This is the first intermolecular carbene transfer from an isolated mono-carbene metal complex into saturated C–H bonds after our previous report of a bis-carbene osmium porphyrin that has a similar reactivity [16].

It is somewhat unexpected that the salen-supported ruthenium carbene complexes **15a–e** are unreactive toward alkene cyclopropanation [21], despite their fairly long Ru=C distances. Treatment of the polypyridine-supported ruthenium carbene complex **16b** with styrene at room temperature for 48 h also results in no appreciable reaction [22].

3. Ruthenium vinylidene and allenylidene complexes supported by macrocyclic amine ligands

3.1. Synthesis

Fourteen ruthenium vinylidene and allenylidene complexes supported by Me_3tacn or 16-TMC ligands have been prepared [38–40]. The synthetic routes to these complexes are depicted in Figs. 14–16.

Treatment of $[(O_2CCF_3)(Me_3tacn)Ru^{II}(PMe_3)_2]PF_6$ with 1 equiv. of HC≡CR (R = Ph, 4-MeC_6H_4) in refluxing 1,2-dichloroethane affords $[(PMe_3)(O_2CCF_3)(Me_3tacn)Ru{=}C{=}CHR]PF_6$ (**17a**, **b**) [38]. Reaction of $[(16\text{-TMC})Ru^{III}Cl_2]Cl$ with HC≡C(C_6H_4X-4) (X = H, Cl, Me, OMe) in refluxing methanol in the presence of zinc amalgam, followed by addition of NH_4PF_6, gives $[Cl(16\text{-TMC})Ru{=}C{=}CH(C_6H_4X\text{-}4)]PF_6$ (**18a–d**) [39]. A similar reaction for $HC{\equiv}CCPh_2OH$, instead of HC≡C(C_6H_4X-4), results in the formation of $[Cl(16\text{-TMC})Ru{=}C{=}CH(CHPh_2)]PF_6$(**19**) [39] (Fig. 14).

The reaction between $[(16\text{-TMC})Ru^{III}Cl_2]Cl$ and $HC{\equiv}CCPh_2OH$ was initially intended as a route to ruthenium allenylidene complex $[Cl(16\text{-TMC})Ru{=}C{=}C{=}CPh_2)]PF_6$ (**20a**) [39]. Possibly, the presence of zinc amalgam throughout the reaction prevents the formation of **20a**. Indeed, when zinc amalgam is removed by filtration after reacting with $[(16\text{-TMC})Ru^{III}Cl_2]Cl$ in refluxing methanol to give the corresponding Ru(II) complex and the filtrate is subsequently treated with $HC{\equiv}CCPh_2OH$ under refluxing conditions, the allenylidene complex **20a** is obtained upon addition of NH_4PF_6. This method has been employed to prepare the allenylidene complexes $[Cl(16\text{-TMC})Ru{=}C{=}C{=}C(C_6H_4X\text{-}4)_2]PF_6$ (**20b–d**) [39] and $[Cl(16\text{-TMC})Ru{=}C{=}C{=}C(py\text{-}2)_2]PF_6$ (**21**) [40] by replacing $HC{\equiv}CCPh_2OH$ with $HC{\equiv}CC(C_6H_4X\text{-}4)_2OH$ and $HC{\equiv}CC(2\text{-py})_2OH$, respectively (Fig. 15).

Interestingly, **21** can function as a "molecular clip", which binds Zn(II) and Ru(II) ions to afford dinuclear complexes $[Cl(16\text{-TMC})Ru{=}C{=}C{=}C(2\text{-py})_2ZnCl_2]PF_6$

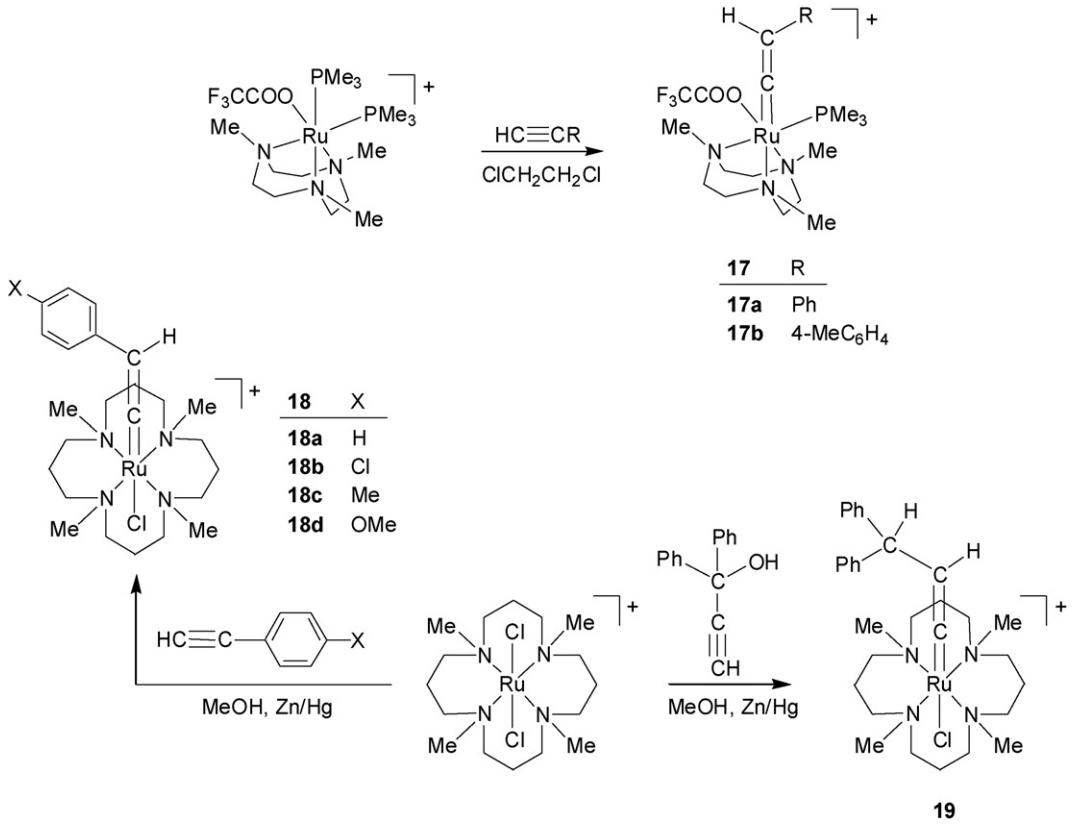

Fig. 14. Synthesis of ruthenium vinylidene complexes **17–19** [38,39] (the PF_6^- counter-anions in these complexes are not shown).

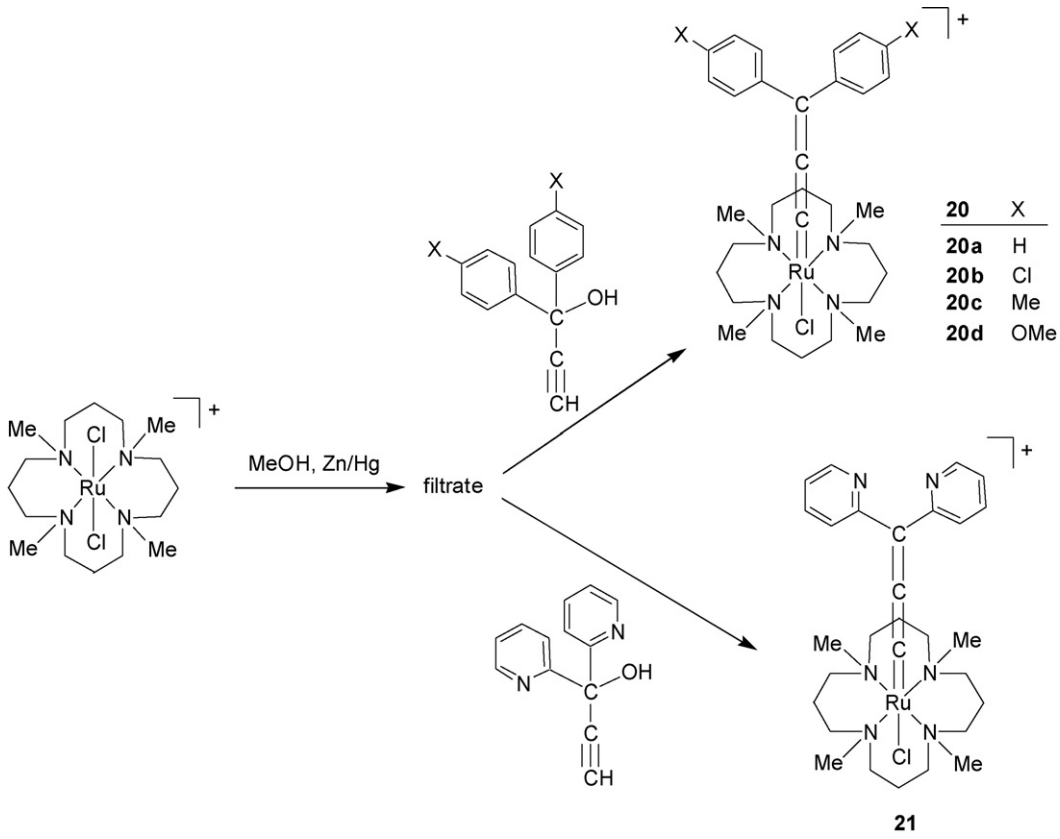

Fig. 15. Synthesis of ruthenium allenylidene complexes **20** and **21** [39,40] (the PF_6^- counter-anions in these complexes are not shown).

(**22**) and [Cl(16-TMC)Ru=C=C=C(2-py)$_2$Ru(acac)$_2$]PF_6 (**23**, acac = acetylacetonate) upon treatment with $ZnCl_2$ and *cis*-[Ru(acac)$_2$(MeCN)$_2$], respectively [40] (Fig. 16).

3.2. Spectroscopic features

IR, ^{13}C NMR and UV–vis absorption spectra of the Me_3tacn- or 16-TMC-supported ruthenium vinylidene and allenylidene complexes have been examined [38–40]. Selected spectroscopic data are compiled in Tables 6 and 7. For comparison, these tables also include the corresponding data of ruthenium vinylidene and allenylidene complexes supported by bis(diphenylphosphino)methane (dppm) [41,42].

The vinylidene complexes **17–19** show ν(CC) bands at 1585–1635 cm^{-1}. These frequencies are considerably lower than that of their dppm counterpart [Cl(dppm)$_2$Ru=C=CHPh]PF_6 (ν(C=C) 1658 cm^{-1}) [41], indicating a strong electron-donating ability of Me_3tacn and 16-TMC. The Ru=C$_\alpha$ signals of **17–19** have chemical shifts of δ 347.4–363.7 ppm, which are substantially downfield from the

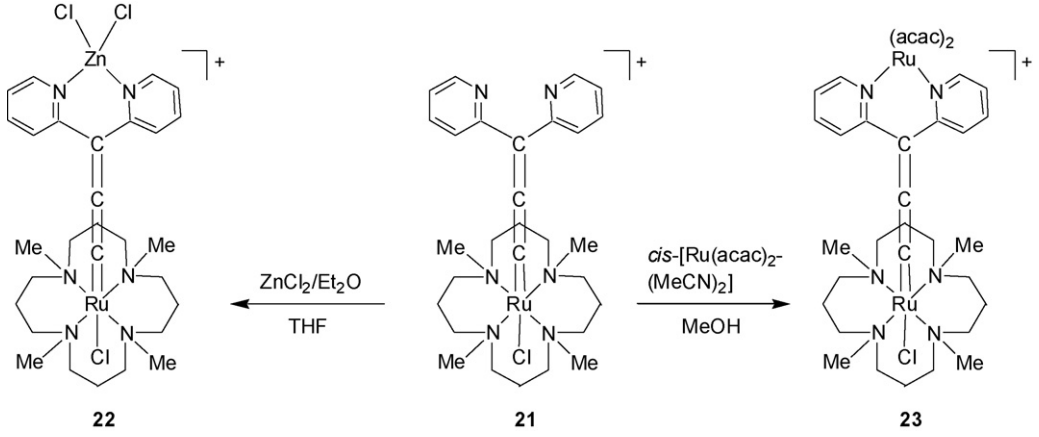

Fig. 16. Synthesis of ruthenium allenylidene complexes **22** and **23** [40] (the PF_6^- counter-anions in these complexes are not shown).

Table 6
Selected IR and ^{13}C NMR spectroscopic data of ruthenium vinylidene ($Ru{=}C_\alpha{=}C_\beta RR'$) and allenylidene ($Ru{=}C_\alpha{=}C_\beta{=}C_\gamma RR'$) complexes supported by Me_3tacn and 16-TMC ligands as compared with those supported by dppm ligands

Complex	ν(C=C)/(C=C=C) (cm^{-1})	^{13}C NMR (δ (ppm))			Ref.
		C_α	C_β	C_γ	
$[(PMe_3)(O_2CCF_3)(Me_3tacn)Ru{=}C{=}CHPh]PF_6$ (**17a**)	1621	363.7 (d)	111.6		[38]
$[(PMe_3)(O_2CCF_3)(Me_3tacn)Ru{=}C{=}CH(C_6H_4Me\text{-}4)]PF_6$ (**17b**)	1635	362.9 (d)	110.8		[38]
$[Cl(16\text{-}TMC)Ru{=}C{=}CHPh]PF_6$ (**18a**)	1593, 1607	349.4, 351.5	111.1, 111.4		[39]
$[Cl(16\text{-}TMC)Ru{=}C{=}CH(C_6H_4Cl\text{-}4)]PF_6$ (**18b**)	1585, 1609	347.4, 349.4	110.2, 110.5		[39]
$[Cl(16\text{-}TMC)Ru{=}C{=}CH(C_6H_4Me\text{-}4)]PF_6$ (**18c**)	1604, 1625	350.5, 352.6	110.9, 111.2		[39]
$[Cl(16\text{-}TMC)Ru{=}C{=}CH(C_6H_4OMe\text{-}4)]PF_6$ (**18d**)	1604, 1624	350.9,353.1	110.6, 110.8		[39]
$[Cl(16\text{-}TMC)Ru{=}C{=}CH(CHPh_2)]PF_6$ (**19**)	1631	347.4, 350.5	112.1, 112.4		[39]
$[Cl(dppm)_2Ru{=}C{=}CHPh]PF_6$	1658	336.02	110.73		[41]
$[Cl(16\text{-}TMC)Ru{=}C{=}C{=}CPh_2]PF_6$ (**20a**)	1884	302.9, 308.6	248.7, 250.7	150.1, 150.7	[39]
$[Cl(16\text{-}TMC)Ru{=}C{=}C{=}C(C_6H_4Cl\text{-}4)_2]\ PF_6$ (**20b**)	1880	300.6, 306.4	255.2, 257.3	149.7, 149.8	[39]
$[Cl(16\text{-}TMC)Ru{=}C{=}C{=}C(C_6H_4Me\text{-}4)_2]PF_6$ (**20c**)	1885	300.0, 305.7	240.9, 242.8	150.1, 150.7	[39]
$[Cl(16\text{-}TMC)Ru{=}C{=}C{=}C(C_6H_4OMe\text{-}4)_2]PF_6$ (**20d**)	1891	294.6, 300.1	229.1, 230.9	149.4, 149.7	[39]
$[Cl(16\text{-}TMC)Ru{=}C{=}C{=}C(2\text{-}py)_2]\ PF_6$ (**21**)	1885	313.4, 319.2	284.8, 287.3	143.0, 143.6	[40]
$[Cl(16\text{-}TMC)Ru{=}C{=}C{=}C(2\text{-}py)_2ZnCl_2]PF_6$ (**22**)	1896	309.2, 312.7	210.0	132.2	[40]
$[Cl(16\text{-}TMC)Ru{=}C{=}C{=}C(2\text{-}py)_2Ru(acac)_2]PF_6$ (**23**)	1871	269.4, 274.8	245.6, 246.6	126.8	[40]
$[Cl(dppm)_2Ru{=}C{=}C{=}CPh_2]PF_6$	1928	306.72 (q)	208.94 (br q)	161.88 (br s)	[42]
$[Cl(dppm)_2Ru{=}C{=}C{=}C(C_6H_4Cl\text{-}4)_2]PF_6$	1921	307.33 (q)	213.92 (br s)	156.63 (br s)	[42]
$[Cl(dppm)_2Ru{=}C{=}C{=}C(C_6H_4Me\text{-}4)_2]PF_6$	1928	301.0	203.0	160.8	[42]

Ru=*C* signals of the ruthenium carbene complexes supported by salen, polypyridine and porphyrin ligands listed in Table 1 (except **7e**).

Compared to **17–19**, the allenylidene complexes **20–22** exhibit markedly upfield $Ru{=}C_\alpha$ signals with δ 294.6–319.2 ppm (which are comparable to those of most of the ruthenium porphyrin carbene complexes). The ν(C=C=C) bands of **20–22** appear at 1880–1896 cm^{-1}. A considerably lower ν(C=C=C) frequency of 1871 cm^{-1} is observed for allenylidene complex **23**; this complex shows substantially upfield $Ru{=}C_\alpha$ signal (δ 269.4 and 274.8 ppm) from those of its analogues **20–22**. Like the case of the vinylidene complexes, all the allenylidene complexes **20–23** have considerably lower ν(C=C=C) frequencies than their dppm counterparts $[Cl(dppm)_2Ru{=}C{=}C{=}CR_2]PF_6$ (R = Ph, 4-ClC_6H_4, 4-MeC_6H_4) (1921–1928 cm^{-1}) [42].

The UV–vis absorption spectra of the vinylidene complexes **18a–d** show similar intense bands ($\varepsilon_{max} \geq 10^4$ dm^3 mol^{-1} cm^{-1}) in the high-energy region ($\lambda_{max} \leq 315$ nm). Appreciably different high-energy bands are observed for **19** wherein the Ru=C=C and phenyl moieties are indirectly connected via a saturated carbon atom (in contrast to the direct attachment of the aryl group to the Ru=C=C moiety in **18**). These absorption bands are suggested to involve the vinylidene moiety [39]. For all the vinylidene complexes **18a–d** and **19**, there are weak low-energy bands appearing at λ_{max} 464–644 nm ($\varepsilon < 10^2$ dm^3 mol^{-1} cm^{-1}), which can be assigned to d–d transitions.

Allenylidene complexes **20a–d** exhibit a low-energy band at λ_{max} 479–513 nm in their UV–vis absorption spectra. This band is intense ($\varepsilon_{max} > 10^3$ dm^3 mol^{-1} cm^{-1}) and attributed to a metal-perturbed intraligand transition with some allenylidene-to-metal LMCT character [39]. On going from **20a–c** to their dppm counterparts $[Cl(dppm)_2Ru{=}C{=}C{=}CR_2]PF_6$ [42], the λ_{max} of the low-energy band red shifts by 1060–1110 cm^{-1}. Complex **21** shows an intense low-energy band (λ_{max} 468 nm, ε 1.9×10^4 dm^3 mol^{-1} cm^{-1}) slightly blue shifted from that of

Table 7
UV–vis spectral data of 16-TMC-supported ruthenium vinylidene and allenylidene complexes in MeCN as compared with those of *trans*-$[Cl(dppm)_2Ru{=}C{=}C{=}CR_2]PF_6$

Complex	λ_{max} (nm) (ε_{max} (dm^3 mol^{-1} cm^{-1}))	Ref.
$[Cl(16\text{-}TMC)Ru{=}C{=}CHPh]PF_6$ (**18a**)	273 (19,700), 311 (7360), 351 (590), 464 (68), 585 (38), 644 (37)	[39]
$[Cl(16\text{-}TMC)Ru{=}C{=}CH(C_6H_4Cl\text{-}4)]PF_6$ (**18b**)	277 (21,510), 315 (12,790), 354 (3250), 470 (78), 578 (48), 638 (46)	[39]
$[Cl(16\text{-}TMC)Ru{=}C{=}CH(C_6H_4Me\text{-}4)]PF_6$ (**18c**)	273 (25,040), 311 (10,740), 350 (900), 464 (68), 582 (33)	[39]
$[Cl(16\text{-}TMC)Ru{=}C{=}CH(C_6H_4OMe\text{-}4)]PF_6$ (**18d**)	273 (28,830), 310 (10,130), 365 (570), 465 (71), 585 (37)	[39]
$[Cl(16\text{-}TMC)Ru{=}C{=}CH(CHPh_2)]PF_6$ (**19**)	237 (22,850), 304 (2200), 395 (83), 466 (82), 589 (br, sh, 21)	[39]
$[Cl(16\text{-}TMC)Ru{=}C{=}C{=}CPh_2]PF_6$ (**20a**)	258 (14,110), 283 (13,160), 335 (7390), 479 (20,200)	[39]
$[Cl(16\text{-}TMC)Ru{=}C{=}C{=}C(C_6H_4Cl\text{-}4)_2]\ PF_6$ (**20b**)	292 (15,360), 335 (9790), 483 (21,740)	[39]
$[Cl(16\text{-}TMC)Ru{=}C{=}C{=}C(C_6H_4Me\text{-}4)_2]PF_6$ (**20c**)	260 (14,780), 291 (12,830), 341 (11,510), 492 (24,430)	[39]
$[Cl(16\text{-}TMC)Ru{=}C{=}C{=}C(C_6H_4OMe\text{-}4)_2]PF_6$ (**20d**)	264 (14,540), 279 (13,370), 382 (17,510), 513 (29,760)	[39]
$[Cl(dppm)_2Ru{=}C{=}C{=}CPh_2]PF_6$	273 (46,900), 357 (9010), 506 (17,120)	[42]
$[Cl(dppm)_2Ru{=}C{=}C{=}C(C_6H_4Cl\text{-}4)_2]PF_6$	274 (49,940), 366 (12,590), 510 (19,970)	[42]
$[Cl(dppm)_2Ru{=}C{=}C{=}C(C_6H_4Me\text{-}4)_2]PF_6$	273 (48,390), 374 (14,170), 519 (20,210)	[42]

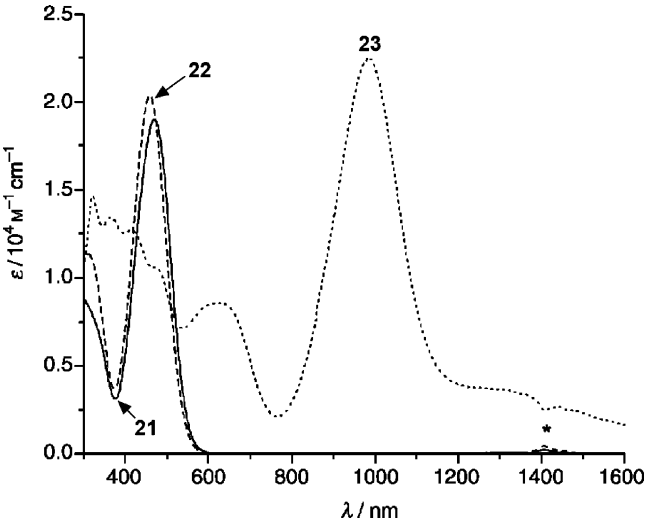

Fig. 17. UV–vis absorption spectra of [Cl(16-TMC)Ru=C=C=C(2-py)$_2$]PF$_6$ (**21**), [Cl(16-TMC)Ru=C=C=C(2-py)$_2$ZnCl$_2$]PF$_6$ (**22**) and [Cl(16-TMC)Ru=C=C=C(2-py)$_2$Ru(acac)$_2$]PF$_6$ (**23**) in MeCN at 298 K (instrumental artefacts are marked by *) [40].

20a, which can also be attributed to a metal-perturbed $\pi \rightarrow \pi^*$ allenylidene intraligand transition. Coordination of **21** to Zn(II) to form **22** further blue shifts the λ_{max} of the intense band to 457 nm (ε 2.0 × 10^4 dm^3 mol^{-1} cm^{-1}).

Strikingly, when **21** binds Ru(II) to form **23**, the lowest-energy band in the UV–vis absorption spectrum dramatically red shifts by ~11,300 cm^{-1}, resulting in the appearance of an intense band at λ_{max} 989 nm (ε 2.3 × 10^4 dm^3 mol^{-1} cm^{-1}) [40] (Fig. 17). Density functional theory (DFT) calculations on model complex [Cl(NH$_3$)$_4$Ru=C=C=C(2-py)$_2$Ru(acac)$_2$]$^+$ suggest that the 989 nm band of **23** should originate from Ru$_{acac}$-to-π*(Ru=C=C=C(2-py)$_2$Ru) charge-transfer transitions, and that the dramatic red shift occurs because (i) the HOMO-1 of **23** is localized on Ru$_{acac}$ (which has a higher energy than the π(Ru=C=C=C(2-py)$_2$) orbital of **21**) and (ii) the LUMO of **23** features a greater delocalization between the two Ru(II) ions [40]. Thus, **23** serves as a unique isolable allenylidene-bridged metal complex showing delocalization across the {M=C=C=C(2-py)$_2$M} moiety in the excited state.

Resonance Raman spectra have been measured for the vinylidene complex **19** and allenylidene complex **20a** [39]. In the case of **19**, the fundamental of the nominal ν(C=C) stretch mode (the largest resonance Raman progression) is located at 1629 cm^{-1}, which generates an overtone at 3258 cm^{-1} and produces combination bands with some fundamental Franck–Condon active modes. The spectrum of **20a** (Fig. 18) shows the fundamental and overtone of the nominal ν(C=C=C) stretch mode as the largest resonance Raman progression at 1889 and 3786 cm^{-1}, respectively, the former of which forms weaker combination bands with eight other fundamental Franck–Condon active modes. Analysis of the resonance Raman spectroscopic data, together with simulation of the 479 nm band and the resonance Raman intensities of **20a**, shows that the 479–513 nm charge-transfer bands of **20a–d** originate from a transition associated with the Ru=C=C=C moiety and are strongly coupled to the allenylidene ligands [39].

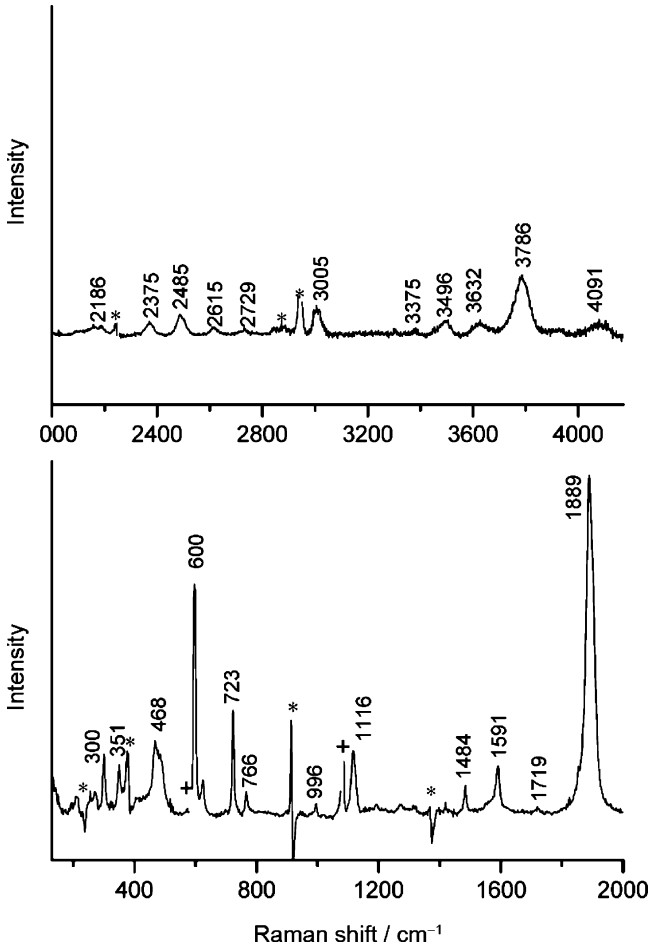

Fig. 18. Resonance Raman spectrum of [Cl(16-TMC)Ru=C=C=CPh$_2$]PF$_6$ (**20a**) in MeCN at 25 °C (excitation wavelength: 435.7 nm). The solvent and laser subtraction artifacts are marked by * and +, respectively [39].

3.3. Structure

16-TMC-supported ruthenium vinylidene complexes **18a** and **19** [39] and allenylidene complexes **20a**, **20c** [39], **22** and **23** [40] have been structurally characterized. Selected bond distances and angles are listed in Table 8. The structures of mononuclear complexes **18a**, **20a** and dinuclear complexes **22** and **23** are shown in Figs. 19 and 20, respectively.

The Ru=C distances in the vinylidene complexes **18a** and **19** are 1.780(8) and 1.802(7) Å, respectively, appreciably shorter than those of almost all the ruthenium porphyrin carbene complexes in Table 2. Both **18a** and **19** have an essentially linear Ru=C=C moiety, with respective Ru–C–C angles of 172.6(7)° and 177.8(6)° and C=C distances of 1.352(10) and 1.309(10) Å. These structural data show that replacing the phenyl group in the vinylidene ligand of **18a** with a diphenylmethyl group slightly lengthens the Ru=C bond but shortens the C=C bond.

For the allenylidene complexes **20a** and **20c**, the Ru=C=C=C moieties are also linear, but their Ru=C distances of 1.849(4) and 1.862(7) Å are considerably longer, whereas the C$_\alpha$=C$_\beta$ distances of 1.262(7) and 1.24(1) Å are markedly shorter, than those of the above two vinylidene complexes. The C$_\beta$=C$_\gamma$ distances in **20a** and **20c** are 1.339(7) and 1.378(10) Å, respectively, longer

Table 8
Selected bond distances and angles of ruthenium vinylidene (Ru=C_α=C_βRR′) and allenylidene (Ru=C_α=C_β=C_γRR′) complexes supported by 16-TMC ligand

Complex	Bond distance (Å)			Bond angle (°)		Ref.
	M=C_α	C_α=C_β	C_β=C_γ	M–C_α–C_β	C_α–C_β–C_γ	
[Cl(16-TMC)Ru=C=CHPh]PF_6 (**18a**)	1.780(8)	1.352(10)		172.6(7)		[39]
[Cl(16-TMC)Ru=C=CH($CHPh_2$)]PF_6 (**19**)	1.802(7)	1.309(10)		177.8(6)		[39]
[Cl(16-TMC)Ru=C=C=CPh_2]PF_6 (**20a**)	1.849(4)	1.262(7)	1.339(7)	177.6(4)	170.1(5)	[39]
[Cl(16-TMC)Ru=C=C=C(C_6H_4Me-4)$_2$]PF_6 (**20c**)	1.862(7)	1.24(1)	1.378(10)	180	180	[39]
[Cl(16-TMC)Ru=C=C=C(2-py)$_2$$ZnCl_2$]$PF_6$ (**22**)	1.835(6)	1.258(8)	1.356(8)	175.6(5)	171.7(6)	[40]
[Cl(16-TMC)Ru=C=C=C(2-py)$_2$Ru(acac)$_2$]PF_6 (**23**)	1.894(6)	1.243(7)	1.380(7)	174.0(5)	175.8(6)	[40]

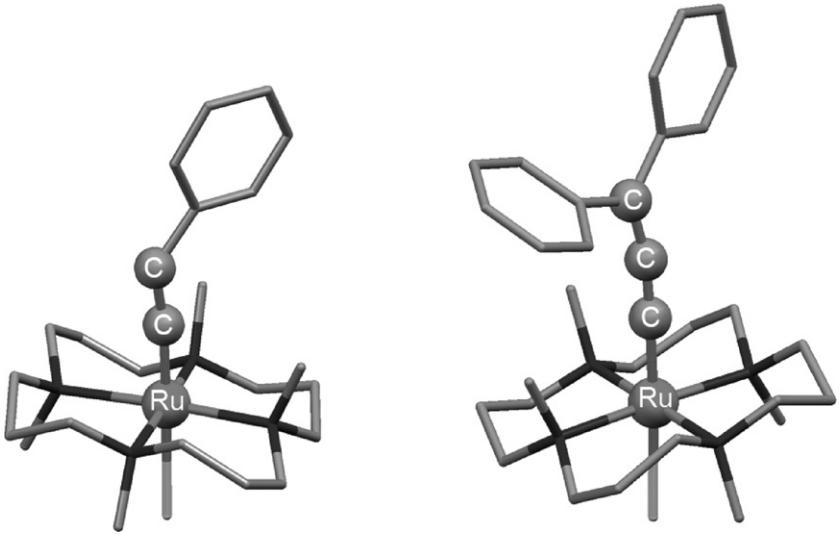

Fig. 19. Structures of [Cl(16-TMC)Ru=C=CHPh]PF_6 (**18a**) and [Cl(16-TMC)Ru=C=C=CPh_2]PF_6 (**20a**) [39].

than the C_α=C_β distances in the same complexes. Similar structural features are observed for the Ru=C=C=C moieties in the dinuclear allenylidene complexes **22** and **23**, although the latter has a slightly longer Ru=C bond than the former.

The bond distances of the Ru=C=C/Ru=C=C=C moieties in the six ruthenium vinylidene/allenylidene complexes supported by 16-TMC ligand are comparable to those in the corresponding complexes supported by other ligands (Ru=C 1.76–1.91 Å

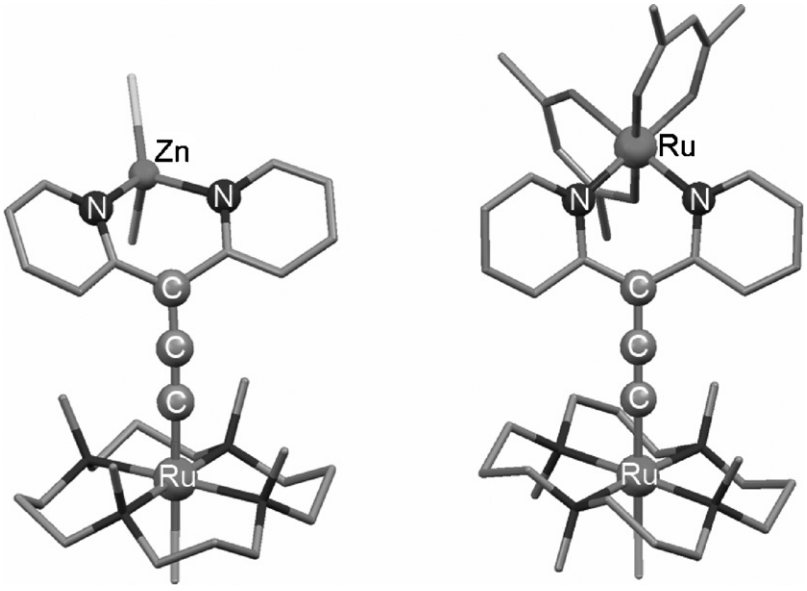

Fig. 20. Structures of [Cl(16-TMC)Ru=C=C=C(2-py)$_2$$ZnCl_2$]$PF_6$ (**22**) and [C1(16-TMC)Ru=C=C=C(2-py)$_2$Ru(acac)$_2$]PF_6 (**23**) [40].

Table 9
Half-wave potentials (V vs. $Cp_2Fe^{+/0}$) of 16-TMC-supported ruthenium vinylidene and allenylidene complexes as compared with those of $[Cl(dppm)_2M{=}C{=}C{=}C(C_6H_4X\text{-}4)_2]PF_6$ (M = Ru, Os)

Complex	$E_{1/2}$		Ref.
$[Cl(16\text{-TMC})Ru{=}C{=}CH(CHPh_2)]PF_6$ (**19**)	0.81[a]	−2.16[b]	[39]
$[Cl(16\text{-TMC})Ru{=}C{=}C{=}CPh_2]PF_6$ (**20a**)	0.64	−1.27	[39]
$[Cl(16\text{-TMC})Ru{=}C{=}C{=}C(C_6H_4Cl\text{-}4)_2]\ PF_6$ (**20b**)	0.70	−1.19	[39]
$[Cl(16\text{-TMC})Ru{=}C{=}C{=}C(C_6H_4Me\text{-}4)_2]PF6$ (**20c**)	0.57	−1.32	[39]
$[Cl(16\text{-TMC})Ru{=}C{=}C{=}C(C_6H_4OMe\text{-}4)_2]PF_6$ (**20d**)	0.49	−1.42	[39]
$[Cl(16\text{-TMC})Ru{=}C{=}C{=}C(2\text{-py})_2]\ PF_6$ (**21**)	0.73[a]	−1.11	[40]
$[Cl(16\text{-TMC})Ru{=}C{=}C{=}C(2\text{-py})_2ZnCl_2]PF_6$ (**22**)	0.96[a]	−0.73	[40]
$[Cl(16\text{-TMC})Ru{=}C{=}C{=}C(2\text{-py})_2Ru(acac)_2]PF_6$ (**23**)[c]	1.01	−1.03	[40]
$[Cl(dppm)_2Ru{=}C{=}C{=}CPh_2]PF_6$	1.02	−0.98	[39]
$[Cl(dppm)_2Ru{=}C{=}C{=}C(C_6H_4Cl\text{-}4)_2]PF_6$	1.06	−0.92	[39]
$[Cl(dppm)_2Ru{=}C{=}C{=}C(C_6H_4Me\text{-}4)_2]PF_6$	0.92	−1.02	[39]
$[Cl(dppm)_2Os{=}C{=}C{=}CPh_2]PF_6$	0.82	−1.14	[39]
$[Cl(dppm)_2Os{=}C{=}C{=}C(C_6H_4Cl\text{-}4)_2]PF_6$	0.88	−1.05	[39]
$[Cl(dppm)_2Os{=}C{=}C{=}C(C_6H_4Me\text{-}4)_2]PF_6$	0.75	−1.20	[39]

[a] Irreversible, $E_{p,a}$.
[b] Irreversible; $E_{p,c}$.
[c] An extra reversible couple at $E_{1/2}$ −0.27 V is observed.

and $C_\alpha{=}C_\beta$ 1.14–1.34 Å for vinylidene complexes; Ru=C 1.84–2.00 Å, $C_\alpha{=}C_\beta$ 1.18–1.27 Å and $C_\beta{=}C_\gamma$ 1.35–1.41 Å for allenylidene complexes) [3b]. A comparison among the structures of **18a**, **20a** and *trans*-[(16-TMC)Ru(C≡CPh)$_2$] (Ru–C 2.077(4) Å, $C_\alpha{\equiv}C_\beta$ 1.198(6) Å) [43] reveals that the Ru=C and $C_\alpha{=}C_\beta$ distances of **20a** both fall in between the corresponding distances of the vinylidene and acetylide complexes, and the $C_\alpha{=}C_\beta$ bond in the allenylidene complex has partial triple bond character.

3.4. Electrochemistry

Electrochemical studies have been performed on **19** [39], **20a–d** [39] and **21–23** [40]. The observed $E_{1/2}$ values, along with those for $[Cl(dppm)_2M{=}C{=}C{=}C(C_6H_4X\text{-}4)_2]PF_6$ (M = Ru, Os) [39], are listed in Table 9. Fig. 21 shows the cyclic voltammograms of **20a**, **21** and **23**.

In the cyclic voltammograms of **20a–d**, a reversible reduction couple at $E_{1/2}$ −1.42 to −1.19 V and a reversible oxidation couple at 0.49–0.70 V are observed, in contrast to the two irreversible waves at $E_{p,c}$ −2.16 and $E_{p,a}$ 0.81 V in the case of **19**. Two reversible couples are also observed for $[Cl(dppm)_2Ru{=}C{=}C{=}C(C_6H_4X\text{-}4)_2]PF_6$, but their $E_{1/2}$ values are 270–380 mV more anodic than those of **20a–d**. The ruthenium allenylidene complexes supported by dppm and 16-TMC ligands both exhibit smaller $E_{1/2}$ values upon increasing the electron-donating strength of the C_6H_4X-4 substituents, and from X = Cl to OMe, a decrease in $E_{1/2}$ by ∼200 mV is noted for **20a–d**.

Changing the phenyl groups in **20a** to 2-pyridyl groups to give **21** causes the oxidation couple to become irreversible and renders the reversible reduction couple 310 mV more anodic. An additional anodic shift of 380 mV of the reversible reduction couple occurs upon coordination of **21** to Zn(II) to give the dinuclear allenylidene complex **22**. For the conversion of **21** into **23**, a markedly smaller anodic shift of 80 mV for the reduction cou-

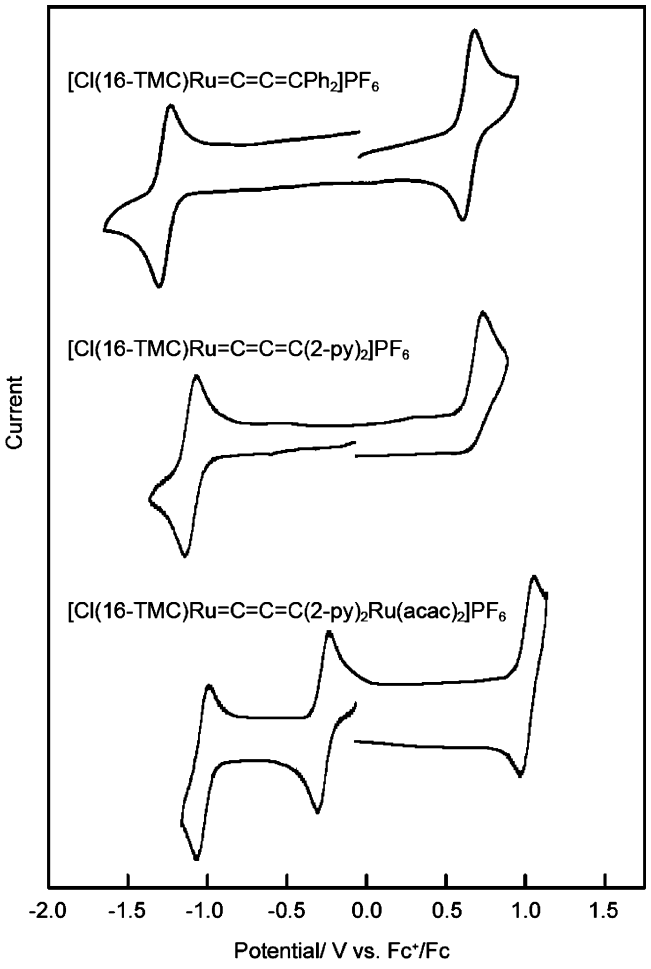

Fig. 21. Cyclic voltammograms of $[Cl(16\text{-TMC})Ru{=}C{=}C{=}CPh_2]PF_6$ (**20a**) [39], $[C1(16\text{-TMC})Ru{=}C{=}C{=}C(2\text{-py})]PF_6$ (**21**) and $[Cl(16\text{-TMC})Ru{=}C{=}C{=}C(2\text{-py})_2Ru(acac)_2]PF_6$ (**23**) in CH_3CN with 0.1 M $^nBu_4NPF_6$ as supporting electrode [40]. Conditions: working electrode, glassy carbon; scan rate, 100 mV s^{-1} (Fc^+/Fc = ferrocenium/ferrocene).

ple is observed, accompanied by a change in the oxidation wave from irreversible to reversible, together with the appearance of an extra reversible couple at $E_{1/2}$ −0.27 V.

The two reversible couples of **20a–d** can be assigned to the electrochemical reactions at the Ru=C=C=CR_2 unit, rather than at the metal or ligand center only, on the basis of the dependence of the $E_{1/2}$ values of the ruthenium allenylidene complexes on both the auxiliary ligand (16-TMC and dppm) and the 4-XC_6H_4 substituent, and by considering the considerably different $E_{1/2}$ values of [Cl(dppm)$_2$M=C=C=C(C_6H_4X-4)$_2$]PF_6 for M = Ru and Os [39]. This assignment is supported by the smaller difference (380 mV) in the $E_{1/2}$ value of the oxidation couple between **20a** and [Cl(dppm)$_2$Ru=C=C=CPh_2]PF_6 than that (740 mV) in $E_{1/2}$($Ru^{III/II}$) between *trans*-[(dppm)$_2$$RuCl_2$] [44] and [(16-TMC)$RuCl_2$] [45], and the large decrease in $E_{1/2}$ value from M = Ru to Os observed for the $M^{III/II}$ couple of *trans*-[(16-TMC)MCl_2] (770 mV) compared with that (200 mV) for the oxidation couple of [Cl(dppm)$_2$M=C=C=CPh_2]$^+$.

A similar assignment may be made for the redox waves of **21**–**23**, except the reversible couple of **23** at −0.27 V, which is assigned to the $Ru^{III/II}$ couple of the {Ru(acac)$_2$} moiety [40]. Such an $E_{1/2}$($Ru^{III/II}$) value of {Ru(acac)$_2$} moiety is similar to that in *cis*-[Ru(acac)$_2$(MeCN)$_2$] (−0.28 V) [40] and *cis*-[Ru(acac)$_2$(pyrazine)$_2$] (−0.29 V) [46]. Since for **23** the oxidation couple of the {Ru(acac)$_2$} moiety lies between the reduction and oxidation couples of the {Cl(16-TMC)Ru=C=C=C(2-py)$_2$}$^+$ unit, this suggests the location of the highest filled electronic level of {Ru(acac)$_2$} in between the π and π* levels of {Cl(16-TMC)Ru=C=C=C(2-py)$_2$}$^+$ in **23**.

3.5. Reactivity

Although the reactions of ruthenium vinylidene or allenylidene complexes with nucleophiles have been extensively studied [1–3], we observed no reaction between the ruthenium allenylidene complexes **20a–d** and MeOH even under refluxing conditions for 48 h, nor were the vinylidene complexes **18a–d** and **19** found to be reactive with refluxing MeOH [39]. Complex **20a** is also unreactive with NaOMe in methanol at room temperature for 48 h. Presumably, both the steric protection provided by the four NMe groups of 16-TMC and the increase in the π-basicity of the ruthenium ion by the pure σ-donor 16-TMC render the $C_α$ atom in these Ru=$C_α$=$C_β$=$C_γ$RR′ or Ru=$C_α$=$C_β$RR′ complexes less susceptible to nucleophilic attack.

For the Me_3tacn-supported ruthenium vinylidene complexes **17a** and **17b** (which are stable in refluxing methanol), their reactions with primary and secondary amines only lead to the deprotonation of the vinylidene ligands [38], unlike the formation of aminocarbene and isocyanide complexes from the reaction of ruthenium vinylidene complexes with primary and secondary amines reported by Bianchini and co-workers [47]. Deprotonation of the C=CHR ligands in **17a** and **17b** with methanolic KOH in the presence of phosphine L gives the σ-acetylide complexes [(PMe_3)(L)(Me_3tacn)Ru–C≡CR]PF_6 [L = PMe_3, P(OMe)$_3$] [38] (reaction 4 in Fig. 22). The resistance of **17a** and **17b** to nucleophilic addition is proposed to result from an electronic rather than steric factor [38].

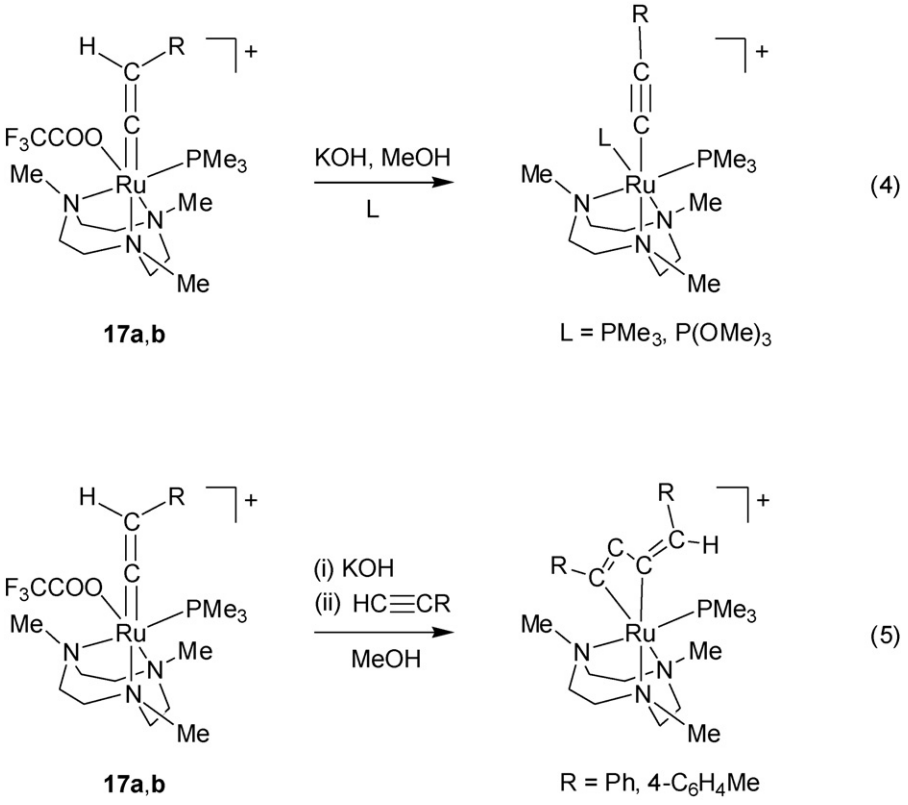

Fig. 22. Reactivity of ruthenium vinylidene complexes supported by Me_3tacn ligand [38].

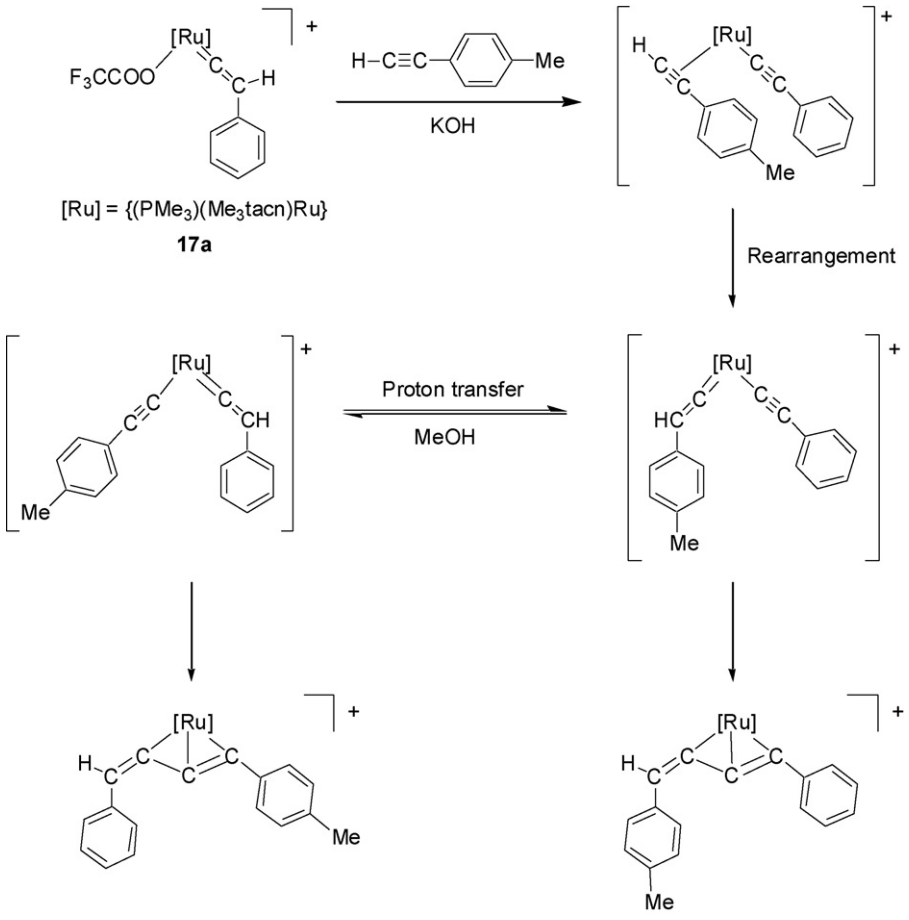

Fig. 23. Proposed mechanism for the formation of $[(PMe_3)(Me_3tacn)Ru\{\eta^3\text{-}(C_6H_4Me\text{-}4)C_3{=}CHPh\}]PF_6$ and $[(PMe_3)(Me_3tacn)Ru\{\eta^3\text{-}PhC_3{=}CH(C_6H_4Me\text{-}4)\}]PF_6$ [38].

Complexes **18a–d** do not undergo deprotonation of their C=CHR groups upon treatment with Et_3N. Such deprotonation occurs only when these allenylidene complexes are treated with a stronger base (e.g. NaOMe) [39].

Oxidative cleavage of the vinylidene group in **17a** is observed upon introducing dioxygen into a 1,2-dichloroethane solution of this complex, affording a ruthenium carbonyl complex, $[(PMe_3)(O_2CCF_3)(Me_3tacn)Ru(CO)]^+$, and benzaldehyde [38]. In solutions open to air, complexes **18a–d** undergo similar oxidative vinylidene cleavage to give a carbonyl complex within 10 h [39].

Alkyne-vinylidene coupling reactions take place when the Ru=C=CHR complexes **17a** and **17b** are sequentially treated with KOH and HC≡CR in refluxing methanol, resulting in the formation of η^3-butenynyl complexes $[(PMe_3)(Me_3tacn)Ru\{\eta^3\text{-}RC_3{=}CHR\}]PF_6$ (R = Ph, 4-MeC_6H_4, respectively) [38] (reaction 5 in Fig. 22). Interestingly, if the substituent in the alkyne is different from that in the vinylidene group, such as the reaction of **17a** with HC≡C(C_6H_4Me-4) in methanolic KOH, a 1:1 mixture of two isomeric η^3-butenynyl complexes $[(PMe_3)(Me_3tacn)Ru\{\eta^3\text{-}(C_6H_4Me\text{-}4)C_3{=}CHPh\}]PF_6$ and $[(PMe_3)(Me_3tacn)Ru\{\eta^3\text{-}PhC_3{=}CH\text{-}(C_6H_4Me\text{-}4)\}]PF_6$ is formed [38]. We proposed that this occurs by a stepwise mechanism shown in Fig. 23, which involves the generation of an (η^2-alkyne)(σ-acetylide) intermediate and its rearrangement to a (vinylidene)(σ-acetylide) intermediate (the latter can isomerize through proton transfer) followed by 1,2-migratory insertion of the coordinated acetylide [38].

The alkyne–vinylidene coupling reactions of **17a** and **17b** are closely related to the alkynyl/alkyne coupling reactions reported for other ruthenium complexes [48], most of which are proposed to involve (vinylidene)(σ-acetylide) intermediates [48b–e,48h]. The reaction of a vinylidene complex, $[(PNP)Cl_2Ru{=}C{=}CH(C_6H_4Me\text{-}4)]$ ($PNP = CH_3CH_2CH_2N(CH_2CH_2PPh_2)_2$), with LiC≡CPh in THF was found, by Bianchini and co-workers [49], to afford $[(PNP)Ru(C{\equiv}CPh)\{\eta^3\text{-}PhC_3{\equiv}CH(C_6H_4Me\text{-}4)\}]$ only, without formation of the isomer $[(PNP)Ru(C{\equiv}CPh)\{\eta^3\text{-}(C_6H_4Me\text{-}4)C_3{\equiv}CHPh\}]$; this is different from the above reaction between the Ru=C=CHPh complex **17a** and HC≡C(C_6H_4Me-4) in methanolic KOH.

4. Concluding remarks

Macrocyclic ligands including porphyrins and tertiary polyamines are good auxiliaries for stabilizing ruthenium- and osmium–carbon multiple bonds. It is practical to use these

nitrogen-containing macrocycles to significantly regulate the electronic/steric properties of the ruthenium/osmium–carbon multiple bonds and therefore alter the structure and reactivity of the corresponding metal–carbon multiple bonded species. The lack of aryl groups in polyamine ligands such as 16-TMC renders these macrocycles "optically transparent" and "electrochemically silent", and ideally suitable for investigating the electronic transitions or redox processes associated with the metal–carbon multiple bonds.

Diazo compounds are useful carbene source for the formation of ruthenium, osmium and iron porphyrin carbene complexes [(Por)M=CRR′], which readily bind coordinating molecules L such as MeIm to give [(L)(Por)M=CRR′]. The isolation of stable dinuclear oxo-bridged metal carbene complexes [{(Por)Os=CPh_2}$_2$(μ-O)], along with the bis-carbene metal complexes [(F_{20}-TPP)Os(=CPh_2)$_2$] discussed in previous review [9], reflects a unique property of osmium in the formation of metal-carbon multiple bonds. On the basis of extensive spectroscopic and electrochemical studies and X-ray structural determinations on ruthenium porphyrin carbene complexes, it is evident that the substituents on carbene and porphyrin ligands and the ligands trans to the carbene groups all can have a considerable influence on the porphyrin-supported Ru=CRR′ bonds. Markedly shorter Ru=C distances are observed in the ruthenium carbene complexes supported by porphyrins than by salen and polypyridine ligands. The M=C distances in ruthenium, osmium and iron porphyrin carbene complexes follow an order of Fe < Ru < Os; however, an order of Ru > Fe > Os is seen for the $E_{1/2}$ values of their metal-centered oxidations. Like the cyclopropanation and C–H bond insertion reactivities of ruthenium/osmium porphyrin carbene complexes reviewed previously [9], iron porphyrin analogues can also undergo similar reactions with alkenes or C–H bonds. What seems somewhat unusual is the inertness of ruthenium salen carbene complexes, which have fairly long Ru=C distances, toward these carbenoid transfer reactions.

Ruthenium vinylidene and allenylidene complexes supported by Me_3tacn and 16-TMC macrocycles can be prepared by using the corresponding alkynes HC≡CR and HC≡CCR_2OH as the vinylidene and allenylidene source, respectively. These ruthenium vinylidene and allenylidene complexes do not undergo nucleophilic addition with methanol, amines or NaOMe, unlike previously reported analogous complexes supported by other ligands. Deprotonation of Ru=C=CHR groups occurs upon attack by KOH or NaOMe. The Me_3tacn-supported Ru=C=CHR complexes can react with KOH and alkynes HC≡CR to afford ruthenium η^3-butenynyl complexes by apparent alkyne–vinylidene coupling.

Functionalization of the allenylidene ligand with 2-pyridine groups makes its ruthenium complex supported by 16-TMC act as a "molecular clip", which can bind metal ions to form interesting dinuclear allenylidene-bridged metal complexes such as [Cl(16-TMC)Ru=C=C=C(2-py)$_2$Ru(acac)$_2$]PF_6, a metal allenylidene complex featuring delocalization across the {M=C=C=C(2-py)$_2$M} moiety in the excited state.

The vinylidene/allenylidene groups in [Cl(16-TMC)Ru=CR_2]PF_6/[Cl(16-TMC)Ru=C=C=CR_2]PF_6 can be considered as neutral ligands, like those in other ruthenium vinylidene/allenylidene complexes reported in the literature. However, there are several lines of evidence in favor of the polarized form $Ru^{\delta+}$[(=C)$_n$$CR_2$]$^{\delta-}$ (n = 1, 2) for the Ru=C=CR_2 or Ru=C=C=CR_2 moieties supported by 16-TMC [39]: (i) As a strongly σ-donating ligand, 16-TMC can better stabilize $M^{\delta+}$[(=C)$_n$$CR_2$]$^{\delta-}$-type species. (ii) Spectroscopic studies signify some extent of charge transfer from allenylidene to metal for the low-energy electronic transition associated with [Cl(16-TMC)Ru=C=C=CR_2]$^+$. (iii) Complexes [Cl(16-TMC)Ru=C=C=CR_2]PF_6 (R ≠ H) are inert toward nucleophilic attack by methoxide. (iv) The Ru atom is more positively charged than the C=C=C chain according to ab initio calculation on model complex [Cl(NH_3)$_4$Ru=C=C=CPh_2]$^+$ [39].

Acknowledgement

This work was supported by the University Grant Council of Hong Kong SAR (Area of Excellence Scheme AoE/P-10/01), the Hong Kong Research Grants Council (HKU 7012/05P), and the University of Hong Kong (Generic Drug Research Program).

References

[1] W.A. Nugent, J.M. Mayer, Metal–Ligand Multiple Bonds, Wiley–Interscience, New York, 1988.
[2] A.F. Hill, in: E.W. Abel, F.G.A. Stone, G. Wilkinson (Eds.), Comprehensive Organometallic Chemistry II, vol. 7, Pergamon, Oxford, 1995, p. 299.
[3] (a) A.B. Antonova, A.A. Inganson, Russ. Chem. Rev. (Engl. Transl.) 58 (1989) 693;
(b) M.I. Bruce, Chem. Rev. 91 (1991) 197;
(c) H. Werner, J. Organomet. Chem. 475 (1994) 45;
(d) D. Touchard, P.H. Dixneuf, Coord. Chem. Rev. 178–180 (1998) 409;
(e) M.P. Doyle, D.C. Forbes, Chem. Rev. 98 (1998) 911;
(f) M.I. Bruce, Chem. Rev. 98 (1998) 2797;
(g) C. Bruneau, P.H. Dixneuf, Acc. Chem. Res. 32 (1999) 311;
(h) M.C. Puerta, P. Valerga, Coord. Chem. Rev. 193–195 (1999) 977;
(i) D. Bourissou, O. Guerret, F.P. Gabbaï, G. Bertard, Chem. Rev. 100 (2000) 39;
(j) J.W. Herndon, Coord. Chem. Rev. 206/207 (2000) 237;
(k) M.A. Sierra, Chem. Rev. 100 (2000) 3591;
(l) J.P. Selegue, Coord. Chem. Rev. 248 (2004) 1543;
(m) S. Rigaut, D. Touchard, P.H. Dixneuf, Coord. Chem. Rev. 248 (2004) 1585;
(n) V. Cadierno, M.P. Gamasa, J. Gimeno, Coord. Chem. Rev. 248 (2004) 1627;
(o) D.A. Valyaev, O.V. Semeikin, N.A. Ustynyuk, Coord. Chem. Rev. 248 (2004) 1679;
(p) H. Werner, Coord. Chem. Rev. 248 (2004) 1693;
(q) H. Katayama, F. Ozawa, Coord. Chem. Rev. 248 (2004) 1703;
(r) G. Maas, Chem. Soc. Rev. 33 (2004) 183;
(s) J.W. Herndon, Coord. Chem. Rev. 250 (2006) 1889;
(t) C. Bruneau, P.H. Dixneuf, Angew Chem. Int. Ed. 45 (2006) 2176.
[4] R.H. Grubbs, Angew. Chem. Int. Ed. 45 (2006) 3760, and references therein.
[5] (a) D.A. Smith, D.N. Reynolds, L.K. Woo, J. Am. Chem. Soc. 115 (1993) 2511;
(b) E. Galardon, P. Le Maux, G. Simonneaux, Chem. Commun. (1997) 927;
(c) M. Frauenkron, A. Berkessel, Tetrahedron Lett. 38 (1997) 7175;
(d) E. Galardon, P. Le Maux, G. Simonneaux, J. Chem. Soc., Perkin Trans. 1 (1997) 2455;

(e) E. Galardon, S. Roué, P. Le Maux, G. Simonneaux, Tetrahedron Lett. 39 (1998) 2333;
(f) Z. Gross, N. Galili, L. Simkhovich, Tetrahedron Lett. 40 (1999) 1571;
(g) E. Galardon, P. Le Maux, G. Simonneaux, Tetrahedron 56 (2000) 615;
(h) G. Simonneaux, E. Galardon, C. Paul-Roth, M. Gulea, S. Masson, J. Organomet. Chem. 617/618 (2001) 360;
(i) C.G. Hamaker, J.-P. Djukic, D.A. Smith, L.K. Woo, Organometallics 20 (2001) 5189;
(j) C. Paul-Roth, F. De Montigny, G. Rethoré, G. Simonneaux, M. Gulea, S. Masson, J. Mol. Catal. A. 201 (2003) 79.

[6] (a) W.-C. Lo, C.-M. Che, K.-F. Cheng, T.C.W. Mak, Chem. Commun. (1997) 1205;
(b) S.-L. Zheng, W.-Y. Yu, C.-M. Che, Org. Lett. 4 (2002) 889;
(c) C.-Y. Zhou, W.-Y. Yu, C.-M. Che, Org. Lett. 4 (2002) 3235;
(d) J.-L. Zhang, H.-B. Zhou, J.-S. Huang, C.-M. Che, Chem. Eur. J. 8 (2002) 1554;
(e) G.-Y. Li, J. Chen, W.-Y. Yu, W. Hong, C.-M. Che, Org. Lett. 5 (2003) 2153;
(f) C.-Y. Zhou, W.-Y. Yu, P.W.H. Chan, C.-M. Che, J. Org. Chem. 69 (2004) 7072;
(g) G.-Y. Li, C.-M. Che, Org. Lett. 6 (2004) 1621.

[7] (a) H. Lang, Angew. Chem. Int. Ed. Engl. 33 (1994) 547;
(b) M. Uno, P.H. Dixneuf, Angew. Chem. Int. Ed. 37 (1998) 1714;
(c) S.K. Hurst, M.P. Cifuentes, J.P.L. Morrall, N.T. Lucas, I.R. Whittall, M.G. Humphrey, I. Asselberghs, A. Persoons, M. Samoc, B. Luther-Davies, A.C. Willis, Organometallics 20 (2001) 4664.

[8] (a) A.P. Sadimenko, Advances in Heterocyclic Chemistry, vol. 81, Academic Press, San Diego, 2001, p. 167;
(b) C. Slugovc, R. Schmid, K. Kirchner, Coord. Chem. Rev. 185/186 (1999) 109;
(c) A. Klose, E. Solari, J. Hesschenbrouck, C. Floriani, N. Re, S. Geremia, L. Randaccio, Organometallics 18 (1999) 360;
(d) L. Bonomo, C. Stern, E. Solari, R. Scopelliti, C. Floriani, Angew. Chem. Int. Ed. 40 (2001) 1449.

[9] C.-M. Che, J.-S. Huang, Coord. Chem. Rev. 231 (2002) 151.

[10] J.P. Collman, P.J. Brothers, L. McElwee-White, E. Rose, L.J. Wright, J. Am. Chem. Soc. 107 (1985) 4570.

[11] L.K. Woo, D.A. Smith, Organometallics 11 (1992) 2344.

[12] Y. Li, J.-S. Huang, G.-B. Xu, N. Zhu, Z.-Y. Zhou, C.-M. Che, K.-Y. Wong, Chem. Eur. J. 10 (2004) 3486.

[13] Y. Li, P.W.H. Chan, N.-Y. Zhu, C.-M. Che, H.-L. Kwong, Organometallics 23 (2004) 54.

[14] G. Simonneaux, F. De Montigny, C. Paul-Roth, M. Gulea, S. Masson, Tetrahedron Lett. 43 (2002) 3685.

[15] Y. Li, J.-S. Huang, Z.-Y. Zhou, C.-M. Che, Chem. Commun. (2003) 1362.

[16] Y. Li, J.-S. Huang, Z.-Y. Zhou, C.-M. Che, J. Am. Chem. Soc. 123 (2001) 4843.

[17] K. Sawano, H. Yuge, T.K. Miyamoto, Inorg. Chim. Acta 358 (2005) 1830.

[18] Y. Li, J.-S. Huang, Z.-Y. Zhou, C.-M. Che, X.-Z. You, J. Am. Chem. Soc. 124 (2002) 13185.

[19] (a) D. Mansuy, M. Lange, J.C. Chottard, P. Guerin, P. Morliere, D. Brault, M. Rougee, J. Chem. Soc. Chem. Commun. (1977) 648;
(b) D. Mansuy, M. Lange, J.C. Chottard, J.F. Bartoli, B. Chevrier, R. Weiss, Angew. Chem. Int. Ed. Engl. 17 (1978) 781.

[20] C.G. Hamaker, G.A. Mirafzal, L.K. Woo, Organometallics 20 (2001) 5171.

[21] G.-Y. Li, J. Zhang, P.W.H. Chan, Z.-J. Xu, N. Zhu, C.-M. Che, Organometallics 25 (2006) 1676.

[22] C.-Y. Wong, M.C.W. Chan, N. Zhu, C.-M. Che, Organometallics 23 (2004) 2263.

[23] S.-W. Lai, K.-K. Cheung, M.C.-W. Chan, C.-M. Che, Angew. Chem. Int. Ed. 37 (1998) 182.

[24] W.-M. Xue, M.C.-W. Chan, Z.-M. Su, K.-K. Cheung, S.-T. Liu, C.-M. Che, Organometallics 17 (1998) 1622.

[25] S. Wada, H. Yuge, T.K. Miyamoto, Acta Cryst. C 59 (2003) m369.

[26] M. Kawai, H. Yuge, T.K. Miyamoto, Acta Cryst. C 58 (2002) m581.

[27] T. Harada, S. Wada, H. Yuge, T.K. Miyamoto, Acta Cryst. C 59 (2003) m37.

[28] A. Klose, E. Solari, C. Floriani, N. Re, A. Chiesi-Villa, C. Rizzoli, Chem. Commun. (1997) 2297.

[29] A. Klose, E. Solari, C. Floriani, S. Geremia, L. Randaccio, Angew. Chem. Int. Ed. 37 (1998) 148.

[30] H. Nishiyama, K. Aoki, H. Itoh, T. Iwamura, N. Sakata, O. Kurihara, Y. Motoyama, Chem. Lett. (1996) 1071.

[31] J.W. Buchler, W. Kokisch, P.D. Smith, in: J.D. Dunitz (Ed.), Struct. Bonding (Berlin), vol. 34, Springer, New York, 1978, p. 79.

[32] J.P. Collman, E. Rose, G.D. Venburg, J. Chem. Soc. Chem. Commun. (1993) 934.

[33] J.-P. Djukic, V.G. Young Jr., L.K. Woo, Organometallics 13 (1994) 3995.

[34] E. Galardon, P. Le Maux, L. Toupet, G. Simonneaux, Organometallics 17 (1998) 565.

[35] C.-M. Che, J.-S. Huang, F.-W. Lee, Y. Li, T.-S. Lai, H.-L. Kwong, P.-F. Teng, W.-S. Lee, W.-C. Lo, S.-M. Peng, Z.-Y. Zhou, J. Am. Chem. Soc. 123 (2001) 4119.

[36] J.R. Wolf, C.G. Hamaker, J.-P. Djukic, T. Kodadek, L.K. Woo, J. Am. Chem. Soc. 117 (1995) 9194.

[37] (a) C.J. Ziegler, K.S. Suslick, J. Am. Chem. Soc. 118 (1996) 5306;
(b) C.J. Ziegler, K.S. Suslick, J. Organomet. Chem. 528 (1997) 83.

[38] S.-M. Yang, M.C.-W. Chan, K.-K. Cheung, C.-M. Che, S.-M. Peng, Organometallics 16 (1997) 2819.

[39] C.-W. Wong, C.-M. Che, M.C.W. Chan, K.-H. Leung, D.L. Phillips, N. Zhu, J. Am. Chem. Soc. 126 (2004) 2501.

[40] C.-W. Wong, G.S.M. Tong, C.-M. Che, N. Zhu, Angew. Chem. Int. Ed. 45 (2006) 2694.

[41] D. Touchard, P. Haquette, N. Pirio, L. Toupet, P.H. Dixneuf, Organometallics 12 (1993) 3132.

[42] D. Touchard, N. Pirio, P.H. Dixneuf, Organometallics 14 (1995) 4920.

[43] M.-Y. Choi, M.C.W. Chan, S. Zhang, K.-K. Cheung, C.-M. Che, K.-Y. Wong, Organometallics 18 (1999) 2074.

[44] N.R. Champness, W. Levason, D. Pletcher, M. Webster, J. Chem. Soc. Dalton Trans. (1992) 3243.

[45] C.-M. Che, K.-Y. Wong, C.-K. Poon, Inorg. Chem. 25 (1986) 1809.

[46] T. Hasegawa, T.C. Lau, H. Taube, W.P. Schaefer, Inorg. Chem. 30 (1991) 2921.

[47] C. Bianchini, M. Peruzzini, A. Romerosa, F. Zanobini, Organometallics 14 (1995) 3152.

[48] (a) G. Jia, A.L. Rheingold, D.W. Meek, Organometallics 8 (1989) 1378;
(b) G. Jia, D.W. Meek, Organometallics 10 (1991) 1444;
(c) Y. Wakatsuki, H. Yamazaki, N. Kunegawa, T. Satoh, J.Y. Satoh, J. Am. Chem. Soc. 113 (1991) 9604;
(d) C. Bianchini, C. Bohanna, M.A. Esteruelas, P. Frediani, A. Meli, L.A. Oro, M. Peruzzini, Organometallics 11 (1992) 3837;
(e) N.W. Alcock, A.F. Hill, R.P. Melling, A.R. Thompsett, Organometallics 12 (1993) 641;
(f) A. Santos, J. López, L. Matas, J. Ros, A. Galán, A.M. Echavarren, Organometallics 12 (1993) 4215;
(g) D.C. Liles, P.F.M. Verhoeven, J. Organomet. Chem. 522 (1996) 33;
(h) M.A.J. Ternorio, M.J. Tenorio, M.C. Puerta, P. Valerga, Organometallics 19 (2000) 1333.

[49] C. Bianchini, P. Innocenti, M. Peruzzini, A. Romerosa, F. Zanobini, Organometallics 15 (1996) 272.